bi-2010-015937

Submitted to Biochemistry, September 30, 2010; Revised November 28, 2010

Participation of Glutamate-354 of the CP43 Polypeptide in the Ligation of Mn and the Binding of Substrate Water in Photosystem II[†]

Rachel J. Service[‡], Junko Yano[§], Iain McConnell[∥,⊥], Hong Jin Hwang[¶], Dimitri Niks[‡], Russ Hille[‡], Tom Wydrzynski[∥], Robert L. Burnap[¶], Warwick Hillier[∥], and Richard J. Debus[‡,*]

[‡]Department of Biochemistry, University of California, Riverside CA 92521,

[§]Physical Biosciences Division, Lawrence Berkeley National Laboratory, Berkeley, CA 94720,

[∥]Research School of Biology, The Australian National University, Canberra, ACT Australia 0200,

[¶]Department of Microbiology and Molecular Genetics, Oklahoma State University, Stillwater, OK 74078,

[†]Support for this work was provided by the National Institutes of Health (GM 076232 to R. J. D.), the National Science Foundation (MCB-0818371 to R. L. B.), the Australian Research Council (FT0990972 to W. H.) and the Department of Energy, Director, Office of Science, Office of Basic Energy Sciences, Chemical Sciences, Geosciences, and Biosciences Division (Contract DE-AC02-05CH11231 to J. Y.).

[⊥]Present Address: Department of Chemistry, Yale University, New Haven, CT 06520

*Author to whom correspondence should be addressed. Phone: (951) 827-3483, Fax: (951) 827-4434, E-mail: richard.debus@ucr.edu

Running Title: Influence of CP43-Glu354 on the Mn_4Ca Cluster in PSII

Footnotes

[1]Abbreviations: Chl, chlorophyll; EDTA, ethylenediaminetetraacetic acid; EPR, electron paramagnetic resonance; EXAFS, extended X-ray absorption fine structure; FTIR, Fourier transform infrared; MES, 2-(N-morpholino)-ethanesulfonic acid; NTA, nitrilotriacetic acid; P_{680}, chlorophyll multimer that serves as the light-induced electron donor in PSII; Pheo, pheophytin; PSII, photosystem II; Q_A, primary plastoquinone electron acceptor; Q_B, secondary plastoquinone electron acceptor; RH, relative humidity; XANES, X-ray absorption near edge structure; Y_Z, tyrosine residue that mediates electron transfer between the Mn_4Ca cluster and $P_{680}^{+\bullet}$, Y_D, second tyrosine residue that can reduce $P_{680}^{+\bullet}$ in PSII.

[2]An X-ray crystallographic structural model of PSII at 1.9 Å was recently reported at the 15th International Congress of Photosythesis in Beijing, China by J.-R. Shen, Y. Umena, K. Kawakami, and N. Kamiya (poster PS6.5). In addition to being obtained at much higher resolution than in previous studies, the diffraction data were obtained with much lower X-ray fluxes in order to minimize radiation-induced reduction of the Mn(III/IV) ions. To a large extent, the coordination modes of the ligating amino acid residues in this model appear to resemble those in the 3.0 Å and 2.9 Å structural models, but the new model's compatibility with the polarized EXAFS studies of single crystals is not known as of this writing.

[3]Multiple numbering systems are in use for CP43 (*25*). The different numbering systems arise because *psbC* (the gene encoding CP43) has an unusual start codon, because CP43 is post-translationally processed at its amino terminus, and because, in *Synechocystis* sp. PCC 6803,

there is a deletion of one residue at position 7 compared to the amino acid sequences of CP43 in other organisms. The numbering system used in this study is the same as that used in the X-ray crystallographic studies (*1, 2, 5*).

[4] Specific L-[1-^{13}C]alanine-labeling of PSII shifts the $\nu_{sym}(COO^-)$ mode of the α-COO^- group of D1-Ala344 by either ~ 19 or ~ 36 cm^{-1} (*31, 33, 34, 66*). It is not yet possible to distinguish between these two possibilities.

[5] The spectrum reported in a preliminary version of this study (*27*) as corresponding to the S_2-*minus*-S_1 FTIR difference spectrum in CP43-E354Q PSII core complexes actually corresponds most closely to the S_3-*minus*-S_2 FTIR difference spectrum. The error arose because of the unusual stability of the S_2 state in the mutant and because the samples examined in ref. *27* were given a pre-flash 5 min before measurement. Consequently, two conclusions stated in ref. *27*, namely that a different Mn ion undergoes oxidation during the S_1 to S_2 transition in the mutant and that different functional groups necessarily give rise to the 1400(–) cm^{-1} and 1588(+) cm^{-1} bands in the wild-type S_2-*minus*-S_1 FTIR difference spectrum, are invalid.

Abstract

In the current X-ray crystallographic structural models of photosystem II, Glu354 of the CP43 polypeptide is the only amino acid ligand of the oxygen-evolving Mn_4Ca cluster that is not provided by the D1 polypeptide. To further explore the influence of this structurally unique residue on the properties of the Mn_4Ca cluster, the CP43-E354Q mutant of the cyanobacterium *Synechocystis* sp. PCC 6803 was characterized with a variety of biophysical and spectroscopic methods, including polarography, EPR, X-ray Absorption, FTIR, and mass spectrometry. The kinetics of oxygen release in the mutant were essentially unchanged from those in wild-type. In addition, the oxygen flash-yields exhibited normal period-four oscillations having normal S state parameters, although the yields were lower, correlating with the mutant's lower steady-state rate (approx. 20% compared to wild-type). Experiments conducted with $H_2{}^{18}O$ showed that the fast and slow phases of substrate water exchange in CP43-E354Q thylakoid membranes were accelerated 8.5- and 1.8-fold, respectively, in the S_3 state compared to wild-type. Purified oxygen-evolving CP43-E354Q PSII core complexes exhibited a slightly altered S_1 state Mn-EXAFS spectrum, a slightly altered S_2 state multiline EPR signal, a substantially altered S_2-*minus*-S_1 FTIR difference spectrum, and an unusually long lifetime for the S_2 state (> 10 hours) in a substantial fraction of reaction centers. In contrast, the S_2 state Mn-EXAFS spectrum was nearly indistinguishable from that of wild-type. The S_2-*minus*-S_1 FTIR difference spectrum showed alterations throughout the amide and carboxylate stretching regions. Global labeling with ^{15}N and specific labeling with L-[1-^{13}C]alanine revealed that the mutation perturbs both amide II and carboxylate stretching modes and shifts the symmetric carboxylate stretching modes of the α-COO^- group of D1-Ala344 (the C-terminus of the D1 polypeptide) to higher frequencies by 3 – 4 cm^{-1} in both the S_1 and S_2 states. The EPR and FTIR data implied that 76 –

82 % of CP43-E354Q PSII centers can achieve the S_2 state and that most of these can achieve the S_3 state, but no evidence for advancement beyond the S_3 state was observed in the FTIR data, at least not in a majority of PSII centers. Although the X-ray absorption and EPR data showed that the CP43-E354Q mutation only subtly perturbs the structure and spin state of the Mn_4Ca cluster in the S_2 state, the FTIR and $H_2{}^{18}O$ exchange data show that the mutation strongly influences other properties of the Mn_4Ca cluster, altering the response of numerous carboxylate and amide groups to the increased positive charge that develops on the cluster during the S_1 to S_2 transition and weakening the binding of both substrate water molecules (or water derived ligands), especially the one that exchanges rapidly in the S_3 state. The FTIR data provide evidence that CP43-Glu354 coordinates to the Mn_4Ca cluster in the S_1 state as a bridging ligand between two metal ions, but provide no compelling evidence that this residue changes its coordination mode during the S_1 to S_2 transition. The $H_2{}^{18}O$ exchange data provide evidence that CP43-Glu354 interacts with the Mn ion that ligates the substrate water molecule (or water-derived ligand) that is in rapid exchange in the S_3 state.

The light-driven oxidation of water in Photosystem II (PSII)[1] produces nearly all of the O_2 on Earth and drives the production of nearly all of its biomass. Photosystem II is an integral membrane protein complex that is located in the thylakoid membranes of plants, algae, and cyanobacteria. It is a homodimer *in vivo*, having a total molecular weight of over 700 kDa. Each monomer consists of at least 20 different subunits and contains over 60 organic and inorganic cofactors including 35 Chl *a* and 12 carotenoid molecules. Each monomer's primary subunits include the membrane spanning polypeptides CP47 (56 kDa), CP43 (52 kDa), D2 (39 kDa), and D1 (38 kDa), and the extrinsic polypeptide PsbO (26.8 kDa). The D1 and D2 polypeptides are homologous and together form a heterodimer at the core of each monomer. Within each monomer, the CP47 and CP43 polypeptides are located on either side of the D1/D2 heterodimer and serve to transfer excitation energy from the peripherally-located antenna complex to the D1/D2 heterodimer, and specifically to the photochemically active Chl *a* multimer known as P_{680} (*1-6*).

The O_2-evolving catalytic site consists of a pentanuclear metal cluster containing four Mn ions and one Ca ion. The Mn_4Ca cluster accumulates oxidizing equivalents in response to photochemical events within PSII and then catalyzes the oxidation of two molecules of water, releasing one molecule of O_2 as a by-product (*7-11*). The Mn_4Ca cluster serves as the interface between single-electron photochemistry and the four-electron process of water oxidation. The photochemical events that precede water oxidation take place in the D1/D2 heterodimer. These events are initiated by the transfer of excitation energy to P_{680} following capture of light energy by the antenna complex. Excitation of P_{680} results in the formation of the charge-separated state, $P_{680}^{\bullet+}Pheo^{\bullet-}$. This light-induced separation of charge is stabilized by the rapid oxidation of $Pheo^{\bullet-}$ by Q_A, the primary plastoquinone electron acceptor, and by the rapid reduction of $P_{680}^{\bullet+}$

by Y_Z, one of two redox-active tyrosine residues in PSII. The resulting $Y_Z^{\bullet}$ radical in turn oxidizes the Mn_4Ca cluster, while $Q_A^{\bullet-}$ reduces the secondary plastoquinone, Q_B. Subsequent charge-separations result in further oxidation of the Mn_4Ca cluster and in the two-electron reduction and protonation of Q_B to form plastoquinol, which subsequently exchanges into the membrane-bound plastoquinone pool. During each catalytic cycle, two molecules of plastoquinol are produced at the Q_B site and the Mn_4Ca cluster cycles through five oxidation states termed S_n, where "n" denotes the number of oxidizing equivalents that are stored (n = 0 – 4). The S_1 state predominates in dark-adapted samples. Most interpretations of Mn-XANES and EPR data have concluded that the S_1 state consists of two Mn(III) and two Mn(IV) ions and that the S_2 state consists of one Mn(III) and three Mn(IV) ions (*11-14*). The S_4 state is a transient intermediate. Its formation triggers the rapid oxidation of the two substrate water molecules, the regeneration of the S_0 state, and the release of O_2.

Refined X-ray crystallographic structural models of PSII are available at 3.5 Å (*1*), 3.0 Å (*2*), and 2.9 Å (*5*). These models, plus less-complete models at somewhat lower resolutions (*15, 16*), provide views of the Mn_4Ca cluster and its ligation environment, including 1 – 2 catalytically-essential Cl^- ions that are located 6 – 7 Å distant. However, there are significant differences between these views. For example, in the 2.9 and 3.0 Å structural models, most of the carboxylate ligands are bidentate and the α-COO^- group of D1-Ala344 (the C-terminus of the D1 polypeptide) ligates the Mn_4Ca cluster, whereas in the 3.5 Å structural model, most of the carboxylate ligands are unidentate and the α-COO^- group of D1-Ala344 ligates *no* metal ion. One reason for these differences is that the resolutions of the diffraction data are limited. A second reason is that the Mn(III/IV) ions of the Mn_4Ca cluster were undoubtedly reduced by X-ray generated radicals to their Mn(II) oxidation states during collection of the X-ray diffraction

data (*17, 18*). This reduction would have disrupted the cluster's Mn-O-Mn bridging moieties and altered Mn-ligand interactions. Consequently, the structures of the Mn_4Ca cluster depicted in the X-ray crystallographic models represent unknown superimpositions of native and disrupted Mn_4Ca clusters, with the metal ions in the latter being retained in the vicinity of their native positions by virtue of the crystals being kept frozen at 100 K during data collection. Importantly, none of the crystallographic structural models is fully compatible with polarized EXAFS studies of single crystals of PSII that were conducted with low X-ray fluxes that minimize photoreduction of the Mn ions (*19*) [2]. Nevertheless, the existing crystallographic studies agree with each other, and with the earlier mutagenesis studies (*20*), on the identity of most of the Mn_4Ca cluster's amino acid ligands. Furthermore, the structure of PSII outside the immediate environment of the Mn_4Ca cluster should be largely unaffected by the radiation-induced reduction of the cluster's Mn ions. Consequently, the existing crystallographic structural models are serving as valuable guides for spectroscopic studies designed to provide insight into the structure, dynamics, and mechanism of the Mn_4Ca cluster throughout its catalytic cycle.

To satisfy the very severe energetic and mechanistic constraints of oxidizing water, the Mn_4Ca cluster's reactivity in each of its oxidation states is tightly controlled by its protein environment. The amino acid residues in this environment choreograph the proton and electron reactions associated with water oxidation and play important roles in the delivery of substrate water and the release of O_2 and protons. In particular, these residues minimize the energetic requirements for water oxidation by coupling the requisite proton and electron extraction reactions (*7, 13, 21, 22*), minimize deleterious side-reactions by preventing unregulated access of water to the Mn_4Ca catalyst (*23*), and minimize oxidative damage by promoting rapid egress of newly formed O_2 (*24*). Understanding the influence on the Mn_4Ca cluster of specific residues in

this environment is crucial to understanding the mechanism of water oxidation in PSII.

This study focuses on Glu354 of the CP43 polypeptide [3]. In all of the current X-ray crystallographic structural models, this residue is depicted as being a ligand to the Mn_4Ca cluster and is the only amino acid ligand of the cluster that is not provided by the D1 polypeptide. In the 3.5 Å model, this residue is a bidentate ligand of a single Mn ion [Mn(3)]. In the 3.0 Å and 2.9 Å models, this residue bridges two Mn ions [Mn(2) and Mn(3)], including the Mn ion that is ligated (in these models) by the α-COO^- group of D1-Ala344, the C-terminus of the D1 polypeptide [Mn(2) in these models]. The CP43-E354Q mutation severely impedes the photoautotropic growth of the cyanobacterium *Synechocystis* sp. PCC 6803 and sharply diminishes its O_2 evolving activity (*26-28*). To better understand the role of CP43-Glu354 in influencing the reactivity of the Mn_4Ca cluster, we have characterized the CP43-E354Q mutant with a variety of biophysical and spectroscopic methods including polarography, EPR, FTIR, XANES, EXAFS, and mass spectrometry, the latter to measure the exchange rates of the two substrate water molecules in the S_3 state. Our results provide evidence that CP43-Glu354 coordinates to the Mn_4Ca cluster as a bridging ligand between two metal ions, in agreement with the 2.9 and 3.0 Å X-ray crystallographic structural models (*2, 5*) and with a recent FTIR study of the same mutant (*28*). However, our FTIR data provide no compelling evidence that this residue changes its coordination mode during the S_1 to S_2 transition, contrary to one of the conclusions of the earlier FTIR study (*28*). Our results also provide evidence that CP43-Glu354 interacts with the Mn ion that ligates the substrate water molecule or water-derived ligand that is in rapid exchange in the S_3 state. A preliminary account of this work has been presented (*27*).

MATERIALS AND METHODS

Construction of Mutant and Propagation of Cultures. The CP43-E354Q mutation was

constructed in the *psbC* gene of *Synechocystis* sp. PCC 6803 and transformed into a host strain of *Synechocystis* that lacks the large extrinsic loop of CP43 and contains a hexahistidine-tag (His-tag) fused to the C-terminus of CP47 [the cloned *psbC* gene was the kind gift of W. F. J. Vermaas (Arizona State University); our strategy for introducing mutations into the large extrinsic loop of CP43 is similar to that described in Ref. *29*; the addition of a His-tag to CP47 has been described previously (*30*)]. The wild-type strain was constructed in an identical manner as the mutant strain except that the transforming plasmid carried no site-directed mutation. Single colonies were selected for ability to grow on solid media containing 5 μg/mL kanamycin monosulfate. Solid media contained 5 mM glucose and 10 μM DCMU. The DCMU and antibiotic were omitted from the liquid cultures. Large-scale liquid cultures (each consisting of three 7 L cultures held in glass carboys) were propagated as described previously (*31*). For the purification of PSII core complexes that had been uniformly labeled with ^{15}N, liquid cultures were propagated in the presence of 10 mM $Na^{15}NO_3$ as the sole nitrogen source (98% ^{15}N enrichment, Cambridge Isotope Laboratories, Andover, MA) (*32*). For the purification of L-[1-^{13}C]alanine-labeled PSII core complexes, liquid cultures were propagated in the presence of 0.5 mM L-[1-^{13}C]alanine (99% ^{13}C enrichment, Cambridge Isotope Laboratories, Andover, MA) (*31, 33, 34*). To verify the integrity of the mutant cultures that were harvested for the purification of thylakoid membranes and PSII core complexes, an aliquot of each culture was set aside and the sequence of the portion of the *psbC* gene that encodes the large extrinsic loop of CP43 was obtained after PCR amplification of genomic DNA (*35*). No trace of the wild-type codon was detected in any of the mutant cultures.

Purification of Thylakoid Membranes. Thylakoid membranes were isolated under dim green light at 4 °C with a procedure (*34*) that was modified from that of Tang & Diner (*36*).

Harvested cells were concentrated and suspended in a buffer containing 1.2 M betaine, 10% (v/v) glycerol, 50 mM MES-NaOH (pH 6.0), 5 mM $CaCl_2$, 5 mM $MgCl_2$, 1 mM benzamidine, 1 mM ε-amino-n-caproic acid, 1 mM phenymethylsulfonyl fluoride, and 0.05 mg/mL DNAse I, then broken by nine cycles of (5 s on/15 min off) in a glass bead homogenizer (Bead-Beater, BioSpec Products, Bartlesville, OK). After separation of unbroken cells and debris by low speed centrifugation, the resulting thylakoid membranes were concentrated by ultracentrifugation (20 min at 40,000 rpm in a Beckman Ti45 rotor) and suspended to a concentration of 1.0–1.5 mg of Chl/mL in a buffer containing 1.2 M betaine, 10% (v/v) glycerol, 50 mM MES-NaOH (pH 6.0), 20 mM $CaCl_2$, 5 mM $MgCl_2$. The concentrated thylakoid membranes were either flash-frozen as 1 mL aliquots in liquid nitrogen and stored at -80 °C, or used immediately for the purification of PSII core complexes.

Purification of PSII core complexes. Isolated oxygen-evolving PSII core complexes were purified under dim green light at 4 °C with Ni-NTA superflow affinity resin (Qiagen, Valentia, CA) as described previously (*34*). For most of the experiments, the purification buffer consisted of 1.2 M betaine, 10% (v/v) glycerol, 50 mM MES-NaOH (pH 6.0), 20 mM $CaCl_2$, 5 mM $MgCl_2$, 50 mM histidine, 1 mM EDTA, and 0.03% (w/v) *n*-dodecyl *β*-D-maltoside. For some of the FTIR experiments described in Figure 8, the betaine was omitted from the cell and thylakoid membrane suspension buffers and from the purification buffer and the concentration of glycerol was increased to 25% (v/v). The purified PSII core complexes were concentrated to ~ 1.0 mg of Chl/mL by ultrafiltration, frozen in liquid N_2, and stored at −196 °C (vapor phase nitrogen).

Flash O_2 Yield and Kinetic Measurements. Measurements were performed with a bare platinum electrode that permits the centrifugal deposition of samples onto the electrode surface (*37*). Before deposition, thylakoid membranes were concentrated by centrifugation and

suspended at ~ 0.8 mg of Chl/mL in 50 mM HEPES-NaOH (pH 7.2), 5 mM $CaCl_2$, 10 mM $MgCl_2$, and 1 M sucrose (*38*). For each measurement, 3.2 µg of Chl were deposited on the platinum surface of the platinum electrode by being centrifuged at 18,000 x g for 10 min in a Sorvall HB-4 swing-out rotor. Samples were given a series of 20 preflashes and then dark-adapted for 10 min prior to the initiation of the measuring flash sequence. Flashes were provided by a xenon flash lamp (6 µs FWHM). The preflash sequence was applied to oxidize PSII centers that may populate the "super-reduced" S_{-1} and S_{-2} states. The 10 min dark-adaptation period was incorporated to allow PSII centers to relax to the S_1 and S_0 states. Polarization of the electrode (0.73 V) was initiated 10 s before the initiation of data acquisition and the measuring flash sequence (15 flashes at a frequency of 4 Hz) was initiated 333 ms after that. Numerical extraction of the S state parameters was performed assuming a four-state model (*39, 40*). The kinetics of O_2 release was estimated from the rising portion of the O_2 signal using the exponential method (*41*).

Preparation of EPR and X-ray Absorption Samples. For the experiments of Figures 3A and 4, samples were concentrated to 7 – 8 mg of Chl/mL with Centricon-100 concentrators, transferred into standard quartz 4 mm OD EPR tubes (Wilmad LabGlass, Buena, NJ), dark adapted for 18 hours at 4 °C, then frozen in liquid nitrogen. For the experiments of Figure 3A, condensed O_2 was purged from the EPR tubes immediately prior to measurement by warming the tubes to 198 K (in dry ice and methanol) and directing a stream of Ar gas over the sample for 10 min in absolute darkness followed by rapid freezing in liquid N_2 (*42*). For the EPR experiments of Figure 3B and for the X-ray absorption measurements (Figures 5 and 6), samples were transferred to a buffer containing 1.2 M betaine, 40% (v/v) glycerol, 50 mM MES-NaOH (pH 6.0), 20 mM $CaCl_2$, 5 mM $MgCl_2$, and 0.03% (w/v) *n*-dodecyl *β*-D-maltoside by

concentrating them to ~ 9 mg of Chl/mL with Centricon-100 concentrators, diluting them 20-fold with a buffer containing 42% (v/v) glycerol, then concentrating them to ~ 11 mg of Chl/mL. The concentrated samples were transferred to lucite sample holders that were designed to fit in both EPR and X-ray cryostats (*43*), dark-adapted for 12 hours at 4 °C followed by six hours at room temperature, then frozen in liquid N_2. For the experiments of Figures 3B and 4, the S_2 state was generated by illuminating samples for 5 min in a non-silvered Dewar at 198 K (dry ice/ethanol) with a focused, heat-filtered, 350-Watt Radiac light source. The samples were then immediately frozen in liquid nitrogen.

EPR Measurements. For the experiments of Figures 3A and 4, continuous-wave EPR spectra were recorded with a Bruker ER 300 EPR spectrometer (Bruker BioSpin Corporation, Billerica, MA) equipped with either a Bruker ER 4116 DM dual mode cavity (parallel mode experiments) or a Bruker ER 4102 ST standard cavity (perpendicular mode experiments) . For these experiments, the sample temperature was controlled with an Oxford ESR900 liquid helium cryostat (Oxford Instruments, Oxfordshire, United Kingdom). For the experiments of Figure 3B, continuous-wave EPR spectra were recorded with a Varian E-109 EPR spectrometer equipped with a standard TE102 cavity. For these experiments, the sample temperature was controlled with a Heli-tran liquid helium cryostat (Air Products, Allentown, PA). Sample manipulations were conducted under dim green light at 4 °C.

Preparation of FTIR Samples. All manipulations were conducted under dim green light at 4 °C. Samples (approx. 70 μg of Chl *a*) were exchanged into FTIR analysis buffer [40 mM sucrose, 10 mM MES-NaOH (pH 6.0), 5 mM $CaCl_2$, 5 mM NaCl, 0.06% (w/v) *n*-dodecyl β-D-maltoside (*32, 44*)] by passage through a centrifugal gel filtration column at 27 x g (*45*). Concentrated samples (approx. 10 μL in volume) were mixed with 1/10 volume of fresh 100 mM

potassium ferricyanide (dissolved in water) to serve as the electron acceptor, spread to a diameter of about 10 mm on a 15 mm diameter BaF_2 window, then dried lightly (until tacky) under a stream of dry nitrogen gas. For experiments in which only the S_2-*minus*-S_1 FTIR difference spectrum was recorded (Figures 8B-8D, 9, and 11), samples were placed in a controlled humidity chamber at 95% RH for 10 min. For experiments in which four successive flashes were applied (Figure 7), 1 μL of 20% (v/v) glycerol (in water) was spotted onto the window, adjacent to the sample, but not touching it to maintain the humidity of the sample in the FTIR cryostat at 99% RH (*46*). A second IR window with a Teflon spacer (0.5 mm thick) was placed over the first and sealed in place with silicon-free high-vacuum grease. The sample was loaded immediately into the FTIR cryostat at 273.0 K or 250.0 K and allowed to equilibrate in darkness for 2 h or 18 h, depending on the experiment. Sample concentrations and thicknesses were adjusted so that the absolute absorbance of the amide I band at 1657 cm^{-1} was 0.7 – 1.1.

Measurement of FTIR Spectra. Mid-frequency FTIR spectra were recorded with a Bruker Equinox 55 spectrometer (Bruker Optics, Billerica, MA) at a spectral resolution of 4 cm^{-1} as described previously (*31, 34, 44, 45, 47*). Flash illumination (~ 20 mJ/flash, ~ 7 ns fwhm) was provided by a frequency-doubled Q-switched Nd:YAG laser [Surelite I (Continuum, Santa Clara, CA)]. After dark adaptation, either four successive flashes were applied with an interval of 96 sec between each (Figure 7) or a single flash was applied (Figures 8, 9, and 11). Two single beam spectra were recorded before the first flash and one single-beam spectrum was recorded starting 0.33 sec after the first and subsequent flashes (for the experiments of Figure 7, 8B, 9, and 11, each single beam spectrum consisted of 800 scans; for the experiments of Figures 8C and 8D, each single beam spectrum consisted of 200 scans). The 0.33 sec delay was incorporated to allow for the oxidation of $Q_A^{\bullet-}$ by the ferricyanide. Difference spectra were

obtained by dividing the single-beam spectrum that was recorded after the *n*th flash by the single-beam spectrum that was recorded immediately before the *n*th flash and the ratio was converted to units of absorption. Each sample was subjected to a single set of four flashes (Figure 7), a single flash (Figures 8B, 9, and 11), or to single flashes spaced by 30 min (Figures 8C and 8D). To improve the signal-to-noise ratio, the difference spectra recorded with multiple samples were averaged.

Measurement of Mn XANES and EXAFS Spectra. X-ray absorption spectroscopy (XAS) was performed at the Stanford Synchrotron Radiation Laboratory (SSRL) on beamline 9-3 and 7-3 at an electron energy of 3.0 GeV with an average current of 85-100 mA. The radiation was monochromatized by a Si(220) double-crystal monochromator. The intensity of the incident X-ray beam was monitored by a N_2-filled ion chamber (I_0) in front of the sample. The monochromator energy was calibrated using a pre-edge peak of $KMnO_4$ (6543.3 eV). These standards were placed between two N_2-filled ionization chambers (I_1 and I_2) after the sample. The X-ray flux at 6.6 keV was at 1 x 10^{13} photons $s^{-1}mm^{-2}$. The monochromator was detuned at 6600 eV to 50% of maximal flux to attenuate the X-ray 2nd harmonic. Samples were kept at a temperature of 10 K in a liquid helium flow cryostat to minimize radiation damage. The procedures for data reduction have been described previously (*48*).

Measurement of Substrate Water Exchange Rates by Mass Spectrometry. Frozen thylakoid samples were thawed and diluted to 0.25 mg/mL Chl in 40 mM MES (pH 6.5), 15 mM $MgCl_2$, 15 mM $CaCl_2$, 10% glycerol, and 1.2 M betaine, with potassium ferricyanide added to 0.5 mM to serve as the electron acceptor. Immediately before measurement, individual samples were prepared in total darkness (visualized by IR goggles) and subjected to a one pre-flash, 10 min dark adaptation period to maximize the concentration of PSII centers in the S_1 state. Flashes

were provided with a xenon flash lamp (FWHM = 5.2 μs). The rapid mixing sample chamber that is interfaced to the spectrometer has been described previously (*49*). Two saturating flashes were applied to poise the sample in the S_3 state, then 25 μL of 95% $H_2{}^{18}O$ was injected rapidly (mixing rate, k_{inj} = 175 s^{-1}) to produce a final ^{18}O enrichment of 12.0 ± 0.5%. A third saturating flash (the turnover flash) was then applied at varying delay times (Δt) after $H_2{}^{18}O$ injection to induce O_2 evolution. Measurements of O_2 evolved (Y_C) as a function of Δt were made at *m/e* = 34 for the mixed labeled $^{16,18}O_2$ using an in line mass spectrometer (Vacuum Generation MM6, Winford, UK). The biphasic plots of Y_C versus Δt at *m/e* = 34 were analyzed as the sum of two exponential functions using the following equation (*50*), revealing fast phase k_2 and slow phase k_1 rate constants for substrate water exchange according to the expression,

$$Y_C = 0.57(1 - \exp(-k_2\, t)) + 0.43(1 - \exp(-k_1\, t))$$

Further details of the data analysis procedures are provided in ref. *49*. No data were recorded at *m/e* = 36 for the double labeled $^{18,18}O_2$ because of the low ^{18}O enrichment and small oxygen signals in the mutant samples.

RESULTS

The light-saturated, steady-state O_2 evolving activity of CP43-E354Q cells was 90 – 100 μmol O_2 (mg of Chl)$^{-1}$ h^{-1} compared to 480 – 500 μmol O_2 (μg of Chl)$^{-1}$ h^{-1} for wild-type cells. The lower rate in mutant cells (18 – 20% compared to wild-type) is consistent with earlier reports (*26, 28*). The light-saturated O_2 evolving activity of purified CP43-E354Q PSII core complexes was 0.52 – 0.70 mmol O_2 (mg of Chl)$^{-1}$ h^{-1} compared to 5.1 – 5.5 mmol O_2 (mg of Chl)$^{-1}$ h^{-1} for wild-type PSII core complexes. The lower activity of the purified mutant PSII core complexes (10 – 14% compared to wild-type) suggests that the Mn_4Ca cluster in the *Synechocystis* CP43-E354Q mutant is somewhat labile.

O_2 Flash Yields and Kinetics of O_2 Release. To further investigate the lower rates of O_2 evolution that are caused by the CP43-E354Q mutation, wild-type and mutant thylakoid membranes were isolated and examined with a bare platinum electrode that permits the centrifugal deposition of samples upon the electrode surface. The pattern of O_2 yields that are produced by the individual flashes in a series of saturating single-turnover flashes provides a measure of the efficiency of the individual S state transitions. The pattern of O_2 flash yields in CP43-E354Q thylakoid membranes (Figure 1) showed the same period-four oscillations that are observed in wild-type membranes, although the amplitudes were much smaller, consistent with the lower steady-state rates of O_2 evolution observed in the mutant cells and PSII core complexes. Analysis of these data revealed that the parameters that describe the factors that contribute to the damping of the oscillations (*i.e.*, the parameters that describe misses, double-hits, and the deactivations that occur in the dark intervals between flashes) are virtually the same in the mutant as in the wild-type control (Table 1). This analysis also revealed that, after a 10 min period of dark-adaptation, the distribution of S states in the mutant thylakoid membranes was only slightly different from that in wild-type: the percentages of PSII centers in the S_1 and S_2 states increased (the latter from 2% to 6%), whereas the percentage in the S_0 state decreased. The kinetics of O_2 release in CP43-E354Q thylakoid membranes in comparison with wild-type are presented in Figure 2. Analysis of these data showed that the kinetics of O_2 release are virtually the same in the mutant as in the wild-type, being characterized by half-times of approximately 1.2 ms.

EPR Spectra. A parallel polarization multiline EPR signal was observed in extensively dark adapted CP43-E354Q PSII core complexes (Figure 3A, lower trace). Between 375 G and 650G, the signal resembled the S_1 state multiline EPR signal observed in wild-type PSII core

complexes (upper trace), in terms of both peak positions and spacings. However, the intensity of the spectrum was low and the features below 375 G and above 650 G could not be obtained reproducibly. A perpendicular polarization multiline EPR signal was observed in extensively dark-adapted CP43-E354Q PSII core complexes after illumination at 195 K (Figure 3B, lower trace). This signal was originally observed *before* illumination in mutant PSII core complexes that had been dark adapted for only 2 h. Further investigation revealed that the signal decayed very slowly at 4 °C (Figure 4), with about 60% of the signal decaying with a half-time of about 2.5 h and the remainder decaying with a half time greater than 20 hours (Figure 4). For the data shown in Figure 3B, the mutant core complexes were dark adapted 12 hours at 4 °C followed by 6 h at room temperature to fully relax the S_2 state before illumination. In terms of peak positions and spacing, this signal resembles the S_2 state multiline EPR signal that is observed in wild-type PSII core complexes (Figure 3B, upper trace). We assign this signal to the S_2 state and conclude that the S_2 state is unusually stable in CP43-E354Q PSII core complexes. The signal's superfine structure is different from that in wild-type, especially above 3500 G, and the peaks in the mutant spectrum are shifted 10 – 20 G to lower field compared to their positions in the wild-type spectrum. No features were evident between 600 and 2000 G in the mutant spectrum (Figure 3B, insert); the broad features observed in this region in the wild-type spectrum may correspond to cytochrome heme groups.

The integrated area of the seven peaks indicated in the mutant S_2 state mulitine EPR spectrum (asterisks in the lower trace of Figure 3B) was approximately 76% of the integrated area of the corresponding peaks in the wild-type spectrum (asterisks in the upper trace of Figure 3). Accordingly, approximately 76% of the CP43-E354Q PSII core complexes were estimated to contain photooxidizable Mn_4Ca clusters on the basis of the EPR data.

To determine if the mutant reaction centers are able to advance beyond the S_2 state, extensively dark-adapted CP43-E354Q PSII core complexes were illuminated at 0ºC in the presence of 0.5 mM phenyl-1,4-benzoquinone as electron acceptor before being rapidly frozen in liquid nitrogen. The illuminated samples exhibited no "split" EPR signal characteristic of the $S_2Y_Z^{\bullet}$ state in PSII preparations that are unable to advance to the S_3 state (*51-54*) (data not shown). This observation implies that a majority of CP43-E354Q PSII core complexes *are* able to advance beyond the S_2 state to the S_3 state.

X-ray Absorption Data. The Mn K-edge XANES spectra of CP43-E354Q PSII core complexes poised in the S_1 and S_2 states were compared with the corresponding spectra of wild-type PSII core complexes (Figure 5). In the mutant core complexes, the S_1 state was prepared by dark-adapting samples for 12 hours at 4 °C followed by six hours at room temperature. The Mn XANES spectra of the mutant core complex in both the S_1 and S_2 states, including the pre-edge features (inserts in Figure 5A and 5B) were similar to those of wild-type. In particular, the S_2 state XANES spectrum of the mutant was identical to that of wild-type. The similarity of the wild-type and CP43-E354Q spectra is most clearly shown by the similarity of the second derivative spectra (Figures 5C and 5D for the S_1 and S_2 states, respectively).

The Mn K-edge EXAFS spectra of CP43-E354Q PSII core complexes poised in the S_1 and S_2 states were also compared with the corresponding spectra of wild-type PSII core complexes (Figure 6). The wild-type and mutant Mn EXAFS spectra in the S_2 state were nearly indistinguishable, whereas small differences were apparent in the EXAFS spectra of the S_1 state.

FTIR Data. The unusual stability of the S_2 state multiline EPR signal in CP43-E354Q PSII core complexes led us to investigate the stability of the S_2 state with FTIR difference spectroscopy. The spectrum induced by a single flash given to dark-adapted PSII core

complexes corresponds predominantly to the S_2-*minus*-S_1 FTIR difference spectrum (*55-58*). In CP43-E354Q PSII core complexes, the difference spectrum that was generated by a single saturating flash given after 18 h of dark adaptation at 273 K could only be fully regenerated by a subsequent flash after a lengthy dark recovery period of at least 10 hours at 273 K. However, most of the features in the difference spectrum were evident after 30 min of dark recovery (data not shown). Slowest to recover were features in the $\nu_{sym}(COO^-)$ region, particularly the positive band at 1363 cm^{-1}. Consequently, the unusually stability of the S_2 state observed in the EPR experiments, and its multiphasic decay, were confirmed with FTIR, although the rates of decay were slower in the EPR samples than in the FTIR samples. Accordingly, most of the FTIR data were collected by dark adapting samples for 18 h at 273 K and subjecting each sample to single set of four excitation flashes. The samples were then discarded. To increase the signal-to-noise ratio of the recorded spectra, 800 scans were recorded after each measuring flash instead of the 100 scans that we employed previously (*31, 44, 45*). Consequently, the time spacing between flashes was 96 s instead of the 10 – 12 s that has been used in most previous FTIR studies of S state turnovers [*e.g.*, (*32, 44, 46*)].

The FTIR difference spectra induced by four successive flashes given to wild-type and CP43-E354Q PSII core complexes at 273 K after 18 h of dark adaptation are compared in Figure 7. As noted in the previous paragraph, the spectra that are induced by the first flash should correspond predominantly to S_2-*minus*-S_1 FTIR difference spectra. When the overall amplitudes of the S_2-*minus*-S_1 FTIR difference spectra were normalized to the extent of flash-induced charge separation in the samples (accomplished by normalizing the mutant and wild-type spectra to the peak-to-peak amplitudes of the negative ferricyanide peak at 2115 cm^{-1} and the positive ferrocyanide peak at 2038 cm^{-1} produced by the oxidation of $Q_A^{\bullet-}$ by the ferricyanide), the

amplitude of the mutant spectrum was found to be approximately 82% of the amplitude of the wild-type spectrum. Accordingly, approximately 82% of the CP43-E354Q PSII core complexes were estimated to contain photooxidizable Mn_4Ca clusters on the basis of the FTIR data.

Because of the long time intervals between flashes (96 s), it was expected that significant fractions of wild-type PSII centers would relax between flashes (from the S_2 state to the S_1 state or from the S_3 state to the S_2 and S_1 states). Consequently, it was expected that the difference spectra induced by the second, third, and fourth flashes applied to wild-type PSII core complexes would represent mixtures of S state transitions. In support of this expectation, the fourth-flash difference spectrum of wild-type resembles the S_0-*minus*-S_3 FTIR difference spectrum that has been observed in previous studies after the *third* flash [*e.g.*, (*32, 44, 46*)], although its amplitude is smaller. Evidently, the long time interval between flashes dampened the period-four oscillations of the wild-type FTIR difference spectra sufficiently that the S_0-*minus*-S_3 FTIR difference spectrum dominates after the fourth flash. Note especially the features at 1544(+) and 1510(-) cm^{-1} and the features between 1440 and 1350 cm^{-1} in the fourth flash spectrum. These features, typically observed in S_0-*minus*-S_3 FTIR difference spectra (*56-58*), partly reverse spectral features that are present in the S_2-*minus*-S_1 and S_3-*minus*-S_2 FTIR difference spectra. In CP43-E354Q PSII core complexes, because of the unusual stability of the S_2 state, the long time intervals between flashes should cause less damping of the FTIR difference spectra. In this regard, it is noteworthy that the second-flash spectrum of CP43-E354Q PSII core particles generally resembles the second-flash spectrum of wild-type and that the third- and fourth-flash difference spectra of the mutant show no hint of spectral features reversing sign from those present in the first- and second-flash spectra.

The features in the third- and fourth-flash spectra of the CP43-E354Q PSII core particles

differ from those in the first-flash spectrum. In particular, note the presence of the positive feature at 1586 cm^{-1} in the first-flash spectrum and its absence in the third- and fourth-flash spectra, the change in appearance of the spectra between 1460 and 1380 cm^{-1} between the first- and third-flash spectra, and the appearance of features at 1375(-), 1362(+), and 1346(-) cm^{-1} in the third-flash spectra. These spectral changes provide evidence that the majority of CP43-E354Q PSII core complexes advance beyond the S_2 state, in agreement with the EPR data described earlier. Importantly, because the third- and fourth-flash difference spectra show no hint of spectral features reversing sign from those present in the first- and second-flash spectra, these data provide no evidence for S state advancement beyond the S_3 state in a majority of CP43-E354Q PSII core particles, although advancement beyond S_3 in a minority of reaction centers (*i.e.*, the approximately 20% that evolve O_2 with normal flash yields and kinetics) would likely escape detection.

Because the second-, third-, and fourth-flash difference spectra represented mixtures of S oxidation states, we focused our attention on the features of the first-flash difference spectra. Because the wild-type and mutant samples were not given a preflash, the first-flash spectra may contain contributions from Y_D•-*minus*-Y_D (*33*). One of the largest features in the Y_D•-*minus*-Y_D FTIR difference spectrum is a negative band at 1703 cm^{-1} (*32, 33, 59, 60*). Because the negative feature at 1704 cm^{-1} in the wild-type first-flash spectrum is not significantly larger than the feature that is usually observed near this frequency in wild-type S_2-*minus*-S_1 FTIR difference spectra (*55-58*), the spectral features of Y_D•-*minus*-Y_D probably make only small contributions to the wild-type and CP43-E354Q first-flash spectra that are shown in Figure 7. However, the first-flash spectrum of the CP43-E354Q PSII core complexes should contain contributions from Y_Z•-*minus*-Y_Z (*31*) because only 76 – 82% of the mutant complexes contain photooxidizable Mn_4Ca

clusters on the basis of our EPR and FTIR data (see above). The larger negative bands at 1702-1703 cm^{-1} in the CP43-E354Q FTIR difference spectra compared to wild-type probably reflect the flash-induced formation of $Y_Z^{\bullet}$ in the fraction of CP43-E354Q PSII reaction centers that lack Mn_4Ca clusters. However, the features of the Y_Z•-*minus*-Y_Z FTIR difference spectrum are relatively small except for positive bands at 1699, 1550, and 1512 cm^{-1} (*31, 61*). Therefore, we conclude that first-flash spectra are dominated by the wild-type and mutant S_2-*minus*-S_1 FTIR difference spectra and that differences between the wild-type and mutant spectra can be attributed to the CP43-E354Q mutation and not to contaminating features of Y_Z•-*minus*-Y_Z.

The S_2-*minus*-S_1 FTIR difference spectra of wild-type and CP43-E354Q PSII core complexes show many differences, especially throughout the symmetric carboxylate stretching [$\nu_{sym}(COO^-)$] region and the overlapping amide II and asymmetric carboxylate stretching [$\nu_{asym}(COO^-)$] regions (Figure 7, top set of traces). The largest differences include substantially diminished negative features at 1747, 1543, and 1522 cm^{-1}, a substantially diminished positive feature at 1504 cm^{-1}, the appearance of large positive features at 1667 cm^{-1} and 1528 cm^{-1}, the appearance of a negative feature at 1570 cm^{-1}, and a variety of peak shifts and/or amplitude changes between 1450 cm^{-1} and 1380 cm^{-1} in the mutant spectrum. These mutation-induced changes are substantially larger than those that are induced by mutations of other residues that have been assigned as Mn ligands in the current X-ray crystallographic structural models [*e.g.*, D1-D170H (*44, 62*), D1-E189Q (*45, 63*), D1-D342N (*31*), and D1-A344G (*33, 64-66*)].

While this work was originally being prepared for submission, another study of the same mutant constructed independently in the same organism was published (*28*). The S_2-*minus*-S_1 FTIR difference spectrum of CP43-E354Q reported in this study differs in many respects from ours. In particular, the mutant spectrum more closely resembles that of wild-type, showing no

significant differences near 1747 or 1543 cm^{-1} and fewer differences in the symmetric carboxylate stretching region between 1450 and 1380 cm^{-1} [see Figure 4 of ref. *28*]. In comparing the two studies, we noticed three procedural differences that stood out. First, we had purified our PSII core complexes in the presence of 1.2 M betaine and 10% (v/v) glycerol, whereas they employed no betaine, instead using 25% (v/v) glycerol. Second, our samples had been dark-adapted for 18 hours, whereas theirs were dark adapted for only 20 min. Third, our samples had been subjected to a single set of illuminating flashes, whereas theirs were flash-illuminated repeatedly, with a 20 min period of dark adaptation between illuminations. Accordingly, we set out to acquire more FTIR data with samples that had been purified in the presence of 25% (v/v) glycerol (and no betaine), with samples that had been subjected to shorter periods of dark adaptation, and with samples that had been illuminated repeatedly after a suitable period of dark adaptation.

We first determined that S_2 state was similarly stabilized in CP43-E354Q PSII core complexes whether they had been purified in the presence of 25% (v/v) glycerol or 1.2 M betaine and 10% (v/v) glycerol. This determination was made by comparing the decay of the S_2 state multiline EPR signal in mutant PSII core complexes purified in the two types of buffer (data not shown). We also determined that the S_2-*minus*-S_1 FTIR difference spectrum of mutant PSII core complexes purified in the presence of 25% (v/v) glycerol appeared to exhibit the same FTIR difference spectra as those purified in the presence of 1.2 M betaine and 10% (v/v) glycerol when examined under the conditions of Figure 7 (*i.e.*, an 18 hour dark adaptation time followed by a single set of flashes, data not shown). Accordingly, we examined the effect of shorter dark adaptation times.

The S_2-*minus*-S_1 FTIR difference spectra of wild-type and CP43-E354Q PSII core

complexes recorded under a variety of conditions are compared in Figure 8. A comparison of wild-type and mutant PSII core complexes that had been purified in the presence of 25% (v/v) glycerol, dark adapted for only two hours, then given a single flash is shown in Figure 8B (the same number of scans were accumulated after the flash as in Figure 7; to obtain a stable dark-*minus*-dark baseline after only two hours of dark adaptation required recording these data at 250 K instead of at 273 K). These data closely resemble the data acquired after an 18 h adaptation (top pair of traces in Figure 7, reproduced in Figure 8A to facilitate comparison). The primary differences are that the large positive feature at 1668 cm^{-1} in the mutant is less prominent and the positive feature at 1509 cm^{-1} is diminished to a larger extent. The other mutation-induced changes to the features at 1747 cm^{-1}, 1569 cm^{-1}, 1543 cm^{-1}, 1528 cm^{-1}, 1522 cm^{-1}, and between 1450 cm^{-1} and 1380 cm^{-1} noted earlier were still evident.

Next, we investigated the effect of repeatedly illuminating samples. For this purpose, wild-type and mutant PSII core complexes were compared after a 2 h dark adaptation time followed by 16 single flashes spaced by 30 min. For these experiments, PSII core complexes were purified in the presence of either 25% (v/v) glycerol (Figure 8C) or 1.2 M betaine and 10% (v/v) glycerol (Figure 8D). The data shown in Figures 8C and 8D closely resemble each other, again showing that the features of the spectra are not determined by the sample purification buffer. These data also closely resemble the data shown in Figure 8B: the positive feature at 1667 cm^{-1} is less prevalent and the positive feature at 1507 cm^{-1} is diminished to a greater extent than in samples dark adapted for 18 h (Figure 8A). The primary difference between the data of Figured 8C and 8D and the samples not subjected to repeated illuminations (Figures 8A and 8B) is a loss of positive intensity at 1364 cm^{-1} and the appearance of a derivative feature at 1370(+)/1359(-) cm^{-1} in the mutant difference spectra. As noted earlier, the 1364 cm^{-1} feature

required ~ 10 h of dark adaptation for full recovery between flashes. We observed that the 1370(+)/1359(-) cm^{-1} derivative feature became increasingly prominent as the flash illuminations increased (data not shown). Consequently, only 16 illuminations were accumulated for the data shown in Figures 8C and 8D.

The data of Figure 8 show that, regardless of sample purification buffer, time of dark adaptation, or whether samples were illuminated once or multiple times, we obtained essentially the same spectral features in the S_2-*minus*-S_1 FTIR difference spectra of wild-type and CP43-E354Q PSII core complexes. Consequently, the reasons for the different features of the spectra in ref. *28* remain unknown. To determine if the features between 1650 and 1450 cm^{-1} correspond to amide or $\nu_{asym}(COO^-)$ modes, both wild-type and CP43-E354Q PSII core particles were uniformly labeled with ^{15}N. A comparison of the mid-frequency S_2-*minus*-S_1 FTIR difference spectra of unlabeled and ^{15}N-labeled wild-type and CP43-E354Q PSII core complexes is shown in Figure 9. The difference spectrum of ^{15}N-labeled wild-type PSII core complexes (Figure 9A, blue trace) closely resembles spectra reported previously for ^{15}N-labeled PSII preparations from spinach (*67*), *Thermosynechococcus elongatus* (*68*) and *Synechocystis* sp. PCC 6803 (*32, 69*). In particular, the bands at 1552(+), 1543(–), 1531(+), and 1522(–) cm^{-1} have previously been identified as amide II modes because all four bands downshift appreciably after global incorporation of either ^{15}N (*32, 68, 69*) or ^{13}C (*32, 68-70*). The large positive band at 1587 cm^{-1} was previously assigned to a $\nu_{asym}(COO^-)$ mode because it is largely insensitive to the global incorporation of ^{15}N (*32, 68, 69*), but downshifts by 30 – 35 cm^{-1} after global incorporation of ^{13}C (*32, 68-70*). Of particular importance to this study, the large positive band at 1509 cm^{-1} appears to consist of overlapping amide II and $\nu_{asym}(COO^-)$ modes (*32, 68, 69*). Similar ^{15}N-induced shifts are observed in CP43-E354Q PSII core complexes (Figure 9B). In particular, the

global incorporation of ^{15}N downshifts the 1667 cm^{-1} feature to 1666 cm^{-1} and downshifts the positive feature at 1551 cm^{-1} to 1537 cm^{-1}. The magnitudes of these shifts (1 cm^{-1} and 14 cm^{-1}, respectively) are consistent with the 1667 and 1551 cm^{-1} features corresponding to amide I and amide II modes, respectively (*32, 68, 69*).

To isolate the vibrational modes altered by the CP43-E354Q mutation and to display them more clearly, wild-type-*minus*-mutant double difference spectra were calculated for the four experimental conditions shown in Figure 8. Included with these double difference spectra (shown in Figure 10) are double difference spectra calculated with ^{15}N-labeled wild-type and mutant PSII core complexes that were examined under two of the experimental conditions (blue traces in Figures 10A and 10C). As shown previously (Figs. 7 and 8), the CP43-E354Q mutation substantially diminishes the negative feature at 1747 cm^{-1}. This feature has recently been assigned to the carbonyl stretching vibration (C=O) of a carboxylic acid residue whose pK_A decreases in response to the S_1 to S_2 transition (*47*). Of particular interest to this study is the large negative band near 1524 cm^{-1} that appears in all of the double difference spectra. Because this band is largely unaltered by the global incorporation of ^{15}N (Figs. 10A and 10C), it must correspond to the $\nu_{asym}(COO^-)$ mode of a carboxylate residue that appears near 1524 cm^{-1} in the S_1 state in wild-type PSII preparations, but that is eliminated by the CP43-E354Q mutation. If the mutation eliminates this mode from the S_1 state, then the mutation must also eliminate it from the S_2 state. Consequently, there should be a corresponding positive peak in the double difference spectrum. It would be tempting to assign the positive feature near 1508 cm^{-1} in the double difference spectra to the $\nu_{asym}(COO^-)$ mode in the S_2 state. Indeed, this assignment was made by the authors of ref. *28*. However, the global incorporation of ^{15}N causes the 1508 cm^{-1} mode to downshift by 13 – 15 cm^{-1} (Figures 10A, C), showing that, although both amide II and

$\nu_{asym}(COO^-)$ modes contribute to the 1504 – 1509 feature in the wild-type S_2-*minus*-S_1 FTIR difference spectra, it is the amide II mode that is altered by the CP43-E354Q mutation, causing it to appear in the double difference spectrum. Nevertheless, because the 1506 – 1508 cm^{-1} feature in the double difference spectra is quite broad, we cannot exclude the possibility that the $\nu_{asym}(COO^-)$ mode of CP43-Glu354 also appears at 1506 – 1508 cm^{-1} in the double difference spectra of the ^{15}N-labeled samples (*e.g.*, see Figure 10C, blue trace at this frequency).

The large number of features present in the double difference spectra (Figure 10) shows that the CP43-E354Q mutation perturbs multiple carboxylate residues. To determine if the mutation perturbs the α-COO^- group of D1-Ala344 at the C-terminus of the D1 polypeptide, the frequency of this mode was determined by specifically labeling wild-type and CP43-E354Q PSII core complexes with L-[1-^{13}C]alanine (*31, 33, 34, 66*). A comparison of the unlabeled and L-[1-^{13}C]alanine-labeled S_2-*minus*-S_1 FTIR difference spectra of wild-type and CP43-E354Q PSII core complexes is shown in Figures 11A and 11B. The positive feature at 1600 cm^{-1} in the L-[1-^{13}C]alanine-labeled CP43-E354Q PSII core particles (Figure 11B) is characteristic of Mn-depleted PSII (*33*) and is consistent with our conclusions that only 76 – 82% of the mutant PSII core complexes contain photooxidizable Mn_4Ca clusters (see above). In Mn-depleted PSII core complexes, the incorporation of [1-^{13}C]alanine produces no changes in the light-*minus*-dark FTIR difference spectrum between 1450 and 1200 cm^{-1} (*33*). Consequently, the [1-^{13}C]alanine-induced changes that are apparent in the $\nu_{sym}(COO^-)$ region of the S_2-*minus*-S_1 FTIR difference spectrum of CP43-E354Q PSII core complexes (Figure 11B) can be attributed to mutant PSII complexes that *contain* Mn_4Ca clusters, and not to PSII complexes that *lack* Mn_4Ca clusters.

To isolate the L-[1-^{13}C]alanine-shifted $\nu_{sym}(COO^-)$ modes and to display them more clearly, the ^{12}C-*minus*-^{13}C double difference spectra of the region between 1380 and 1280 cm^{-1} in

the wild-type and mutant samples are presented in Figure 11C. The data show that the positions of the L-[1-^{13}C]alanine-shifted modes are shifted 3 – 6 cm^{-1} to higher frequency in both the S_1 and S_2 states in CP43-E354Q PSII core complexes compared to their positions in wild-type, showing that the α-COO$^-$ group of D1-Ala344 is perturbed by the CP43-E354Q mutation [4].

Substrate water exchange data. The results of ^{18}O exchange measurements conducted with wild-type and CP43-E354Q thylakoid membranes poised in the S_3 state are shown in Figure 12. The data revealed the biphasic kinetics that have been observed in all other PSII preparations and that are characteristic of the two substrate water binding sites (*49, 71-75*). The wild-type (black circles) and CP43-E354Q (red circles) data are presented in Figure 12 along with the exchange kinetics, fit according to Equation 1 and depicted with solid lines. The extracted rate constants are listed in Table 2. The inset to Figure 12 shows a shorter time scale to better compare the kinetics of the fast phase. The exchange rate constants for the wild-type thylakoids were $k_1 = 0.47 \pm 0.04$ s^{-1} and $k_2 = 19.7 \pm 1.3$ s^{-1} for the slow and fast phases, respectively. The exchange rates for the CP43-E354Q thylakoids were $k_1 = 0.86 \pm 0.35$ s^{-1} and $k_2 = 167 \pm 38$ s^{-1} for the slow and fast phases, respectively. The most striking impact of the CP43-E354Q mutation is its profound acceleration of the fast exchange rate. The CP43-E354Q mutation accelerated the fast phase of substrate water exchange, k_2, by a factor of 8.5 ± 2.0 and accelerated the slow phase, k_1, by a factor of 1.8 ± 0.8. Evidently, both substrate-binding sites are perturbed by the mutation and both interact more weakly with substrate water in the mutant in the S_3 state compared to wild-type. However, the profound acceleration in the fast phase underlies a far more significant perturbation to the substrate water site that is in rapid exchange.

DISCUSSION

Our observation that CP43-E354Q thylakoid membranes evolve O_2 with normal S state parameters and release kinetics shows that, in at least a fraction of CP43-E354Q PSII reaction centers, the S state transitions proceed normally. This fraction was estimated to be about 20% on the basis of the steady state rate of O_2 evolution in CP43-E354Q cells and the amplitudes of the O_2 flash yields in CP43-E354Q thylakoid membranes. In contrast, between 76% and 82% of the purified CP43-E354Q PSII core complexes contain photooxidizable Mn_4Ca clusters, as estimated on the basis of the amplitude of the mutant S_2 state multiline EPR signal and the amplitude of the mutant S_2-*minus*-S_1 FTIR difference spectrum. Although both the EPR and FTIR data provide evidence that a majority of CP43-E354Q PSII reaction centers advance beyond the S_2 state, the FTIR data provide no evidence that a substantial fraction advances beyond the S_3 state. We conclude that the CP43-E354Q PSII reaction centers are heterogeneous, with a minority able to evolve O_2 with normal S state parameters and O_2 release kinetics and a majority capable of achieving the S_3 state, but unable to advance beyond the S_3 state. Evidence for heterogeneity was also provided by the decay kinetics of the S_2 state. In the EPR samples, the S_2 state multiline EPR signal decayed with approximate half-times of ~ 2.5 h and > 20 h, respectively. In the FTIR samples, the decay times were much faster, with the S_2 state decaying within 30 min in most PSII reaction centers, but requiring up to 10 hours in others. We presume that the difference in decay kinetics in the EPR and FTIR samples reflects differences in the illumination protocols employed for generating the S_2 state and/or differences in the buffers employed for the two sets of measurements. It should be noted that a recent study of an independently constructed CP43-E354Q mutation in *Synechocystis* sp. PCC 6803 reported no apparent heterogeneity (*28*). However, the characterizations reported in that study did not

include measurements of O_2 flash yields and is unclear if the delayed luminescence data would have been sensitive to a small (~ 20%) fraction of Mn_4Ca clusters that evolve O_2 with normal S state parameters.

What could be the reason for the heterogeneity our CP43-E354Q PSII reaction centers? Proton-coupled electron transfer processes are believed to provide the driving force for oxidizing the Mn_4Ca cluster in its higher oxidation states (*7-10*). Recent models postulate that CP43-Arg357 (or D1-Asp61) serves as a redox-activated catalytic base that facilitates the oxidation of the Mn_4Ca cluster during the S_2 to S_3 and S_3 to S_4 transitions (*7, 13, 21, 22, 76-79*). In these models, the formation of $Y_Z^{\bullet}$ when the Mn_4Ca cluster is in its S_2 or S_3 states triggers the deprotonation of CP43-Arg357 (or D1-Asp61) to the thylakoid lumen. Deprotonation to the lumen is necessary from energetic considerations (*80*) and takes place via a network of protonatable amino acid side chains and water molecules such as those envisaged to exist in the potential proton egress channels that have been identified in the X-ray crystallographic structural models (*1, 5, 81-84*). Kinetically efficient proton transfer through these channels requires finely tuned pK_a differences between key residues and transient formation of clusters of water molecules (*80, 85-87*). An alteration of these pK_a values may slow oxidation of the Mn_4Ca cluster in the same manner that mutations that impair proton uptake also slow the transfer of an electron from $Q_A^{\bullet-}$ to $Q_B^{\bullet-}$ in reaction centers of *Rhodobacter sphaeroides* (*88-90*) and the reduction of O_2 to H_2O in cytochrome *c* oxidase (*91-93*). The heterogeneity of CP43-E354Q may arise from a mutation-induced alteration of the pK_a value(s) of one or more key residues that alters the static or dynamic properties of a network of hydrogen bonds that comprises part of a dominant proton egress channel.

A mutation-induced alteration of a network of hydrogen bonds in the vicinity of the Mn_4Ca cluster is evident from the S_2-*minus*-S_1 FTIR difference spectrum of CP43-E354Q PSII core complexes. The data, obtained under a variety of conditions (Figure 10), show that the mutation substantially diminishes or eliminates the negative feature at 1747 cm^{-1} that was recently assigned to a carboxylate group whose pK_a decreases during the S_1 to S_2 transition (*47*). This carboxylate group participates in a network of hydrogen bonds that extends at least 20 Å across the lumenal face of the Mn_4Ca cluster and includes D1-Asp61, D1-Glu65, D1-Glu329, and D2-Glu312, and presumably also includes the Cl ion that is coordinated by D2-Lys317 (*47*). The near or complete elimination of the negative feature at 1747 cm^{-1} suggests that CP43-Glu354 participates in the same network and shows that the CP43-E354Q mutation disrupts the network sufficiently that, in at least a majority of PSII reaction centers, the structural perturbations associated with the S_1 to S_2 transition are no longer transmitted to the carboxylate group that gives rise to the 1747 cm^{-1} band.

An unusually stable S_2 state is also characteristic of PSII preparations that have been depleted of Ca in the presence of the flexible poly-carboxylic acids EDTA, EGTA, or citrate (*94-97*). The inability of these Ca-depleted PSII preparations to advance beyond the $S_2Y_Z^{\bullet}$ state, and the unusual stability of the S_2 state in these preparations, has been attributed to the participation of the Ca ion in the network of hydrogen bonds that facilitates the oxidation of the Mn_4Ca cluster in its higher oxidation states (*98, 99*). Consequently, the unusually stability of the S_2 state in CP43-E354Q PSII core complexes may also reflect a mutation-induced alteration to the pK_a values of residues involved in the deprotonation reactions that facilitate oxidation of the Mn_4Ca cluster in its higher oxidation states.

The small differences between the wild-type and mutant Mn-XANES and Mn-EXAFS

spectra show that the geometric structure and electronic characteristics of the Mn_4Ca cluster are only subtly perturbed by the CP43-E354Q mutation. The light-driven assembly of the Mn_4Ca cluster involves the binding and photooxidation of a single Mn(II) ion to Mn(III), followed by protein structural rearrangements that create or increase the affinity of the binding sites for the additional Mn(II) ions and the Ca ion (*100, 101*). After these ions bind, the Mn ions are photooxidized to their Mn(III/IV) oxidation states characteristic of the physiological S states. Evidently, the elimination of a negatively charged glutamate residue at position 354 of the CP43 polypeptide has little effect on the cluster's ability to assemble and to achieve its native conformation, at least in the S_1 and S_2 states. In contrast, the D1-H332E mutation of *Synechocystis* sp. PCC 6803 substantially alters both the geometric structure and electronic characteristics of the Mn_4Ca cluster, shifting the Mn K-edge energy to a lower energy and elongating the Mn-Mn and Mn-ligand interactions to a far greater extent than are caused by any biochemical treatment (*e.g*, removal of Ca, exchange of Sr for Ca, or inhibition with NH_3) (*102*). In the case of the D1-H332E mutation, these substantial alterations were interpreted in terms of a negatively charged carboxylate oxygen replacing the τ histidyl nitrogen of D1-His332 as a ligand to a Mn(III) or Mn(IV) ion (*102*). In the case of the CP43-E354Q mutation, because of the insensitivity of the Mn-XANES and Mn-EXAFS to the mutation, it remains an open question whether the carboxylate oxygen(s) of Glu354 is(are) replaced by the carbonyl oxygen and/or amine nitrogen of Gln or by one (or two) small molecule(s) (*e.g*., water), or if the Mn ion(s) become(s) coordination deficient in the mutant.

The similarity of the S_2 state multiline EPR signals of wild-type and CP43-E354Q PSII core complexes also shows that the mutation has little effect on the structure or electronic properties of the Mn_4Ca cluster in the S_2 state. The small differences between the appearance of

the wild-type and mutant spectra show that the magnetic interactions that give rise to the S_2 state multiline EPR signal (*103-105*) are only subtly altered by the CP43-E354Q mutation. In contrast, both the *Synechocystis* D1-H332E mutation (*30, 106*) and the substitution of Sr for Ca (*e.g.*, refs. *34* and *107*) substantially perturb these interactions and substantially alter the appearance of the S_2 state multiline EPR signal. The spectral features of the mutant S_1 state multiline EPR signal below 375 G and above 650 G could not be obtained reproducibly. Consequently, it cannot be concluded that the signal is the same as in wild-type. Nevertheless, the similarity of the wild-type and mutant spectra between 375 and 650 G in terms of both peak positions and spacings suggests that the magnetic interactions that give rise to this signal are also only subtly altered by the CP43-E354Q mutation.

Our FTIR data show that the CP43-E354Q mutation introduces far more perturbations into the environment of the Mn_4Ca cluster that than are introduced by mutations that have been constructed at other putative cluster ligands such as D1-Asp170 (*44, 62*), D1-Glu189 (*45, 63*), D1-Asp342 (*31*), and the α-COO^- group of D1-Ala344 (*33, 64-66*). In particular, the S_2-*minus*-S_1 FTIR difference spectrum of CP43-E354Q PSII core complexes showed alterations throughout the amide II, $\nu_{asym}(COO^-)$ and $\nu_{sym}(COO^-)$ regions. This was true whether the PSII core complexes were purified in the presence of 1.2 M betaine or 25% (v/v) glycerol, whether the samples were dark adapted for 18 h or 2 h, or whether the samples were illuminated only once or repeatedly with 30 min of dark adaptation between flashes. Global labeling with ^{15}N showed that the CP43-E354Q mutation perturbs both amide II and carboxylate stretching modes. Specific labeling with L-[1-^{13}C]alanine showed that the CP43-E354Q mutation shifts the $\nu_{sym}(COO^-)$ mode of the α-COO^- group of D1-Ala344 to higher frequencies by 3 – 6 cm^{-1} in both the S_1 and S_2 states. These data are an indication that the CP43-E354Q mutation perturbs

multiple carboxylate groups in the vicinity of the Mn_4Ca cluster. Because the $\nu_{sym}(COO^-)$ mode of the α-COO^- group of D1-Ala344 downshifts in frequency during the S_1 to S_2 transition to approximately the same extent in both wild-type and CP43-E354Q PSII core complexes, these data also show that the same Mn ion undergoes oxidation during the S_1 to S_2 transition in the mutant as in wild-type [5].

As noted earlier, the S_2-*minus*-S_1 FTIR difference spectrum of CP43-E354Q PSII core complexes that was published recently by Shimada et al. (*28*) has fewer differences with wild-type than our mutant spectrum. Because our wild-type and mutant S_2-*minus*-S_1 FTIR difference spectra were essentially the same regardless of sample purification buffer, time of dark adaptation, or whether the samples were illuminated once or multiple times, the reasons for the differences between the spectra presented in ref. (*28*) and the current study remain unknown. In ref. *28*, the four largest features in the wild-type-*minus*-mutant double difference spectrum were assigned to the $\nu_{asym}(COO^-)$ and $\nu_{sym}(COO^-)$ modes of CP43-E354Q on the basis of their insensitivity to D_2O/H_2O exchange (*28*). In that study, the negative features at 1525 cm^{-1} and 1394 cm^{-1} were assigned to the $\nu_{asym}(COO^-)$ and $\nu_{sym}(COO^-)$ modes of CP43-E354Q in the S_1 state, respectively, and the positive features at 1502 cm^{-1} and 1431 cm^{-1} were assigned to the $\nu_{asym}(COO^-)$ and $\nu_{sym}(COO^-)$ modes of CP43-E354Q in the S_2 state, respectively (*28*). On the basis of these assignments, CP43-Glu354 was proposed to bridge two Mn ions in the S_1 state and shift to chelating bidentate coordination of a single Mn ion in the S_2 state (*28*).

However, we consistently observed more features in the $\nu_{sym}(COO^-)$ region of our double difference spectra than the authors of ref. *28*. In particular, our double difference spectra contain an extra pair of bands at 1406(+) and 1416(–) cm^{-1} that are as intense as those at 1429(+) and 1395(–) cm^{-1}. Consequently, we were unable to uniquely assign a particular $\nu_{sym}(COO^-)$ mode

to CP43-Glu354 in either the S_1 or S_2 states. In addition, we could not identify the $\nu_{asym}(COO^-)$ mode of CP43-Glu354 in the S_2 state. Although the authors of ref. *28* assigned a positive feature at 1502 cm^{-1} to this mode, we observed that the corresponding feature in our double difference spectra (appearing at 1506 – 1508 cm^{-1}) downshifted by 14 – 15 cm^{-1} after global labeling with ^{15}N, consistent with the assignment of this feature to an amide II mode but incompatible with the assignment of this feature to a carboxylate mode. Because the 1506 – 1508 cm^{-1} feature is quite broad, we cannot exclude the possibility that the $\nu_{asym}(COO^-)$ mode of CP43-Glu354 appears at this frequency and underlies the amide II mode in the double difference spectrum of the ^{15}N-labeled samples. However, a more straightforward interpretation of our ^{15}N data is that the positive feature at 1506 – 1508 cm^{-1} in our double difference spectrum corresponds solely to an amide II mode. This would imply that the $\nu_{asym}(COO^-)$ mode of CP43-Glu354 in the S_2 state appears elsewhere in the spectrum and is obscured by the amide II or $\nu_{asym}(COO^-)$ mode of another residue that is perturbed by the mutation.

Our data show that the CP43-E354Q mutation eliminates a $\nu_{asym}(COO^-)$ mode at 1524 cm^{-1} from the wild-type S_2-*minus*-S_1 FTIR difference spectrum. We assign this mode to the $\nu_{asym}(COO^-)$ mode of CP43-Glu354 in the S_1 state, in agreement with the authors of ref. *28*. The presence of this mode in the S_2-*minus*-S_1 FTIR difference spectrum of wild-type shows that the carboxylate group of CP43-Glu354 is perturbed by the electrostatic influences that arise from the positive charge that develops on the Mn_4Ca cluster during the S_1 to S_2 transition. The elimination of this mode by the CP43-E354Q mutation is consistent with ligation of the Mn_4Ca cluster by CP43-Glu354. This conclusion is in agreement with the authors of ref. *28* and supports a recent prediction made on the basis of QM/MM calculations that CP43-Glu354 ligates

along the Jahn-Teller axis of a Mn(III) ion and that its $\nu_{asym}(COO^-)$ mode shifts during the S_1 to S_2 transition (*22, 78*).

The frequencies of the $\nu_{asym}(COO^-)$ and $\nu_{sym}(COO^-)$ modes in metal–carboxylate complexes, and the difference in frequency between them, $\Delta\nu$, vary significantly with the metal ion and the type of carboxylate coordination (*108-112*). The $\nu_{sym}(COO^-)$ and $\nu_{asym}(COO^-)$ modes of free ionic Glu and Asp residues generally appear near 1402 – 1404 cm^{-1} and between 1556 and 1579 cm^{-1}, respectively, corresponding to $\Delta\nu$ = 152 – 177 cm^{-1} (*113-116*). Indeed, having $\Delta\nu \approx 160$ cm^{-1} is typical of free ionic carboxylates. Unidentate ligation of a metal ion generally shifts the $\nu_{sym}(COO^-)$ and $\nu_{asym}(COO^-)$ modes to lower and higher frequencies, respectively, increasing $\Delta\nu$ to more than 200 cm^{-1} (*108-112*). Bidentate chelating coordination (characterized by both carboxylate oxygens ligating a single metal ion) generally shifts the $\nu_{sym}(COO^-)$ and $\nu_{asym}(COO^-)$ modes to *higher* and *lower* frequencies, respectively, resulting in $\Delta\nu$ < 100 cm^{-1} (*108-112*). Bidentate bridging ligation (characterized by the carboxylate group bridging two metal ions) can shift the $\nu_{sym}(COO^-)$ and $\nu_{asym}(COO^-)$ modes in either direction and typically results in $\Delta\nu$ being similar to the values found in free ionic carboxylates (*108-112*). Because the $\nu_{asym}(COO^-)$ mode of CP43-Glu354 appears at ~ 1524 cm^{-1} in the S_1 state, a frequency much lower than that of free ionic Asp and Glu residues, our data are inconsistent with unidentate coordination of CP43-Glu354 to a single metal ion, at least in the S_1 state. If the $\nu_{sym}(COO^-)$ of CP43-Glu354 in the S_1 state corresponds to one of the negative bands observed at 1416, 1395, or 1351 cm^{-1} in our wild-type-*minus*-mutant double difference spectra, then our data would be most consistent with CP43-Glu354 bridging two metal ions, such as depicted in the 3.0 and 2.9 Å crystallographic structural models (and in the recently announced 1.9 Å structural model – see footnote 2). Consequently, our data support the conclusion of ref. *28* that CP43-

Glu354 serves a as a bridging ligand between two Mn ions. However, because we cannot attribute the positive feature at 1506 – 1508 cm^{-1} in our double difference spectra to the $\nu_{asym}(COO^-)$ mode of CP43-Glu354 in the S_2 state and cannot uniquely assign specific $\nu_{sym}(COO^-)$ modes to CP43-Glu354, we cannot confirm another conclusion of ref. *28*, that CP43-Glu354 residue changes its coordination mode during the S_1 to S_2 transition. We would note that ^{15}N labeling is more reliable than D_2O/H_2O exchange for differentiating amide II from $\nu_{asym}(COO^-)$ modes because ^{15}N labeling does not rely on D_2O replacing H_2O in all regions of an assembled protein complex.

One of the most striking results of the FTIR studies on PSII to date is the stunning insensitivity of the individual FTIR difference spectra to the mutation of at least three of the Mn_4Ca cluster's six putative carboxylate ligands. Not only do mutations of D1-Asp170 (*44, 62*), D1-Glu189 (*45, 63*), and D1-Asp342 (*31*) fail to eliminate any carboxylate vibrational stretching modes, they fail to produce significant changes in polypeptide backbone conformations as shown by the lack of significant mutation-induced alterations to the amide I and amide II regions of the spectra. Whereas some of the features in the S_{n+1}-*minus*-S_n FTIR difference spectra of PSII clearly correspond to first coordination sphere ligands (*i.e.*, CP43-Glu354 and the α-COO^- group of D1-Ala344), the majority of these features evidently correspond to residues in the cluster's second coordination sphere and beyond and reflect the response of the protein to the positive charge that develops on the Mn_4Ca cluster during the S_1 to S_2 transition [*e.g.*, see ref. *47*] and to the structural changes that are associated with the S_2 to S_3, S_3 to S_0, and S_0 to S_1 transitions.

The exchange rates of the rapidly exchanging and slowly exchanging substrate water molecules in the S_3 state were increased 8.5-fold and 1.8-fold in CP43-E354Q thylakoid membranes, respectively. These results show that the CP43-E354Q mutation weakens the

binding of both substrate water molecules to their respective binding sites in the S_3 state, especially that of the more rapidly exchanging substrate water molecule. The 8.5-fold acceleration is the largest perturbation to the rapid exchange rate yet observed in any system. In earlier work, we considered whether the substrate water molecule in fast exchange was kinetically limited by (i) substrate diffusion into/out of the catalytic site, or (ii) metal ligand exchange (*49, 50, 75, 117*). Either possibility would be kinetically tenable, with the former possibility implying rapid ligand exchange followed by kinetically limiting substrate accessibility. Conversely, the substrate water molecule in slow exchange was argued to be kinetically limited by metal ligand exchange. Recent molecular dynamics simulations of water diffusion in PSII provide evidence that substrate entry takes place many orders of magnitude faster than the measured rates of substrate water exchange (*118*). Consequently, the measured exchange rates for both substrate water molecules must reflect metal-ligand oxygen exchange rates. The rates of metal ligand exchange depend on many factors including the charge and ionic radius of the metal ion, the electronic occupancy of the *d* orbitals, the degree of protonation of the bound water molecule, and the degree of protonation of neighboring ligands (*75, 117*). Despite our limited knowledge of these factors with respect to the Mn_4Ca cluster in PSII, the fact that the CP43-E354Q mutation substantially perturbs the exchange rate of the rapidly exchanging substrate water molecule provides strong evidence that CP43-Glu354 interacts with a substrate water-derived ligand in the S_3 state. Whether this interaction is direct or indirect remains unclear. If the interaction is direct (*i.e.*, if CP43-Glu354 coordinates to the Mn ion that binds the substrate water that is in fast exchange), then the Mn-oxygen bond must be weakened by the change in Mn ligation produced by the CP43-E354Q mutation. If the interaction is indirect, (*i.e.*, if CP43-Glu354 interacts with a substrate water molecule on a different metal ion via one or more

hydrogen bonds), then the metal-oxygen bond must be weakened because of changes to the hydrogen bonds that connect the water molecule to CP43-Glu354. Both possibilities are potentially feasible and both imply a close association of the substrate water-derived oxygen ligand with CP43-Glu354. On the basis of earlier estimates of substrate water-metal bond strengths derived from an analysis of Arrhenius parameters with transition state theory (*50*), the 8.5-fold increase in exchange rate corresponds to an approximately 5.3 kJ/mol decrease in the barrier to ligand exchange, corresponding to a 14% decrease in the total predicted bond enthalpy. A change in predicted bond enthalpy of this magnitude can readily be accommodated by a change in the first coordination sphere of a metal ion; for example, replacing Glu with Gln could produce either *cis* or *trans* ligand effects on a substrate water molecule or water-derived ligand such as a μ-oxo bridge (*75, 119*). It might also be accommodated by a change in the second coordination sphere (*i.e.*, to the hydrogen bonds that interact with the substrate water molecule), but we are unaware of any documented examples of this in the inorganic literature.

The identification of water molecules coordinated to Mn or Ca in high resolution X-ray crystallographic structural models of PSII (*e.g.*, see footnote 2) would be highly significant because two of these water molecules may ultimately provide the substrate oxygen atoms for the O-O bond. Mass spectrometry studies of $H_2{}^{18}O$-exchange have shown that both substrate water molecules are already bound in the S_2 state and that these are bound in different chemical forms or environments (*e.g.*, to different metal ions) (*50, 120*). However, the precise chemical nature of this water molecule (*i.e.*, whether it corresponds to a terminal water molecule, to a water-derived metal ligand such as a terminal hydroxo or oxo species, or to a μ-oxo bridge between two metal ions) remains to be established, although a terminal species has been advocated on the basis of rate constants and activation energies (*50, 75*). The final unresolved question central to

the chemistry of water oxidation is whether both substrate oxygen atoms correspond to the terminal water molecules detected in FTIR studies (*121-123*), or if at least one corresponds to a μ-oxo bridge between two Mn ions, as proposed on the basis of pulsed EPR studies employing ^{17}O and ^{2}H (*124, 125*).

Our discovery, that the CP43-E354Q mutation perturbs the substrate water molecule (or water-derived ligand) that is in fast exchange complements the data presented in the recent FTIR study of Shimada et al. (*28*). The authors of this study examined the weakly H-bonded O-H stretching region of the S_2-*minus*-S_1 FTIR difference spectrum of wild-type and CP43-E354Q PSII particles and concluded that a water molecule binds to same Mn ion that is ligated by CP43-Glu354, although an indirect interaction via hydrogen bonds was not excluded. Our mass spectrometry data are consistent with these results and additionally show that the water molecule detected in ref. *28* and in earlier FTIR studies (*120, 121*) corresponds to a substrate water molecule. One interesting aspect of our ^{18}O exchange measurements is that the substantially accelerated rates of substrate water exchange in the S_3 state have no apparent effect on the S state parameters or O_2 release kinetics that were measured polarographically. This lack of correlation implies that the binding affinities of the substrate water molecules in the S_3 state do not factor in the rate limiting step of O-O bond formation.

SUMMARY AND CONCLUSIONS

Mutant CP43-E354Q PSII reaction centers are heterogeneous, with a minority able to evolve O_2 with normal S state parameters and O_2 release kinetics and a majority capable of achieving the S_3 state, but unable to advance beyond the S_3 state. Although both EPR and X-ray absorption data show that the CP43-E354Q mutation only subtly perturbs the structure and

electronic properties of the Mn_4Ca cluster in the S_1 and S_2 states, FTIR and $H_2{}^{18}O$ exchange data show that CP43-Glu354 interacts with the Mn_4Ca cluster sufficiently that the CP43-E354Q mutation perturbs numerous amide and carboxylate stretching modes and weakens the binding of both substrate water molecules, especially the one that exchanges rapidly. Our FTIR data provide evidence that CP43-Glu354 coordinates to the Mn_4Ca cluster in the S_1 state as a bridging ligand between two metal ions, but provide no compelling evidence that this residue changes its coordination mode during the S_1 to S_2 transition. Our $H_2{}^{18}O$ exchange data additionally provide evidence that CP43-Glu354 interacts with the Mn ion that ligates the substrate water molecule (or water-derived ligand) that undergoes rapid exchange in the S_3 state.

ACKNOWLEDGEMENTS

The authors are grateful to Anh P. Nguyen for maintaining the mutant and wild-type cultures of *Synechocystis* sp. PCC 6803 and for purifying the thylakoid membranes that were used for measurements or for the isolation of PSII core complexes and to V. S. Batista, G. W. Brudvig, V. L. Pecoraro, T. Noguchi, and V. K. Yachandra for stimulating discussions.

REFERENCES

1. Ferreira, K. N., Iverson, T. M., Maghlaoui, K., Barber, J., and Iwata, S. (2004) Architecture of the Photosynthetic Oxygen-Evolving Center, *Science 303*, 1831-1838.
2. Loll, B., Kern, J., Saenger, W., Zouni, A., and Biesiadka, J. (2005) Towards Complete Cofactor Arrangement in the 3.0 Å Resolution Structure of Photosystem II, *Nature 438*, 1040-1044.
3. Kern, J., Biesiadka, J., Loll, B., Saenger, W., and Zouni, A. (2007) Structure of the Mn_4-Ca Cluster as Derived from X-ray Diffraction, *Photosyn. Res. 92*, 389-405.
4. Barber, J. (2008) Crystal Structure of the Oxygen-Evolving Complex of Photosystem II, *Inorg. Chem. 47*, 1700-1710.
5. Guskov, A., Kern, J., Gabdulkhakov, A., Broser, M., Zouni, A., and Saenger, W. (2009) Cyanobacterial Photosystem II at 2.9-Å Resolution and the Role of Quinones, Lipids, Channels, and Chloride, *Nature Struct. & Mol. Biol. 16*, 334-342.
6. Guskov, A., Gabdulkhakov, A., Broser, M., Glöckner, C., Hellmich, J., Kern, J., Frank, J., Müh, F., Saenger, W., and Zouni, A. (2010) Recent Progress in the Crystallographic Studies of Photosystem II, *ChemPhysChem 11*, 1160-1171.
7. McEvoy, J. P. and Brudvig, G. W. (2006) Water-Splitting Chemistry of Photosystem II, *Chem. Rev. 106*, 4455-4483.
8. McCarrick, R. M. and Britt, R. D. (2008) Current Models and Mechanism of Water Splitting, in *Photosynthetic Protein Complexes* (Fromme, P., Ed.) pp 107-136, Wiley-VCH Verlag GmbH & Co. KGaA, Weinheim, Germany.

9. Rappaport, F. and Diner, B. A. (2008) Primary Photochemistry and Energetics Leading to the Oxidation of the $(Mn)_4Ca$ Cluster and to the Evolution of Molecular Oxygen in Photosystem II, *Coord. Chem. Rev. 252*, 259-272.

10. Renger, G. and Renger, T. (2008) Photosystem II: The Machinery of Photosynthetic Water Splitting, *Photosynth. Res. 98*, 53-80.

11. Yano, J. and Yachandra, V. K. (2008) Where Water is Oxidized to Dioxygen: Structure of the Photosynthetic Mn_4Ca Cluster from X-ray Spectroscopy, *Inorg. Chem. 47*, 1711-1726.

12. Yano, J. and Yachandra, V. K. (2007) Oxidation State Changes of the Mn_4Ca Cluster in Photosystem II, *Photosynth. Res. 92*, 289-303.

13. Dau, H. and Haumann, M. (2008) The Manganese Complex of Photosystem II in its Reaction Cycle - Basic Framework and Possible Realization at the Atomic Level, *Coord. Chem. Rev. 252*, 273-295.

14. Sauer, K., Yano, J., and Yachandra, V. K. (2008) X-ray Spectrsocopy of the Photosynthetic Oxygen-Evolving Complex, *Coord. Chem. Rev. 252*, 318-335.

15. Murray, J. W., Maghlaoui, K., Kargul, J., Ishida, N., Lai, T.-L., Rutherford, A. W., Sugiura, M., Boussac, A., and Barber, J. (2008) X-ray Crystallography Identifies two Chloride Binding Sites in the Oxygen Evolving Centre of Photosystem II, *Energy Environ. Sci. 1*, 161-166.

16. Kawakami, K., Umena, Y., Kamiya, N., and Shen, J.-R. (2009) Location of Chloride and its Possible Functions in Oxygen-Evolving Photosystem II Revealed by X-ray Crystallography, *Proc. Natl. Acad. Sci. USA 106*, 8567-8572.

17. Yano, J., Kern, J., Irrgang, K.-D., Latimer, M. J., Bergmann, U., Glatzel, P., Pushkar, Y., Biesiadka, J., Loll, B., Sauer, K., Messinger, J., Zouni, A., and Yachandra, V. K. (2005) X-ray Damage to the Mn_4Ca Complex in Single Crystals of Photosystem II: A Case Study for Metalloprotein Crystallography, *Proc. Natl. Acad. Sci. USA 102*, 12047-12052.

18. Grabolle, M., Haumann, M., Müller, C., Liebisch, P., and Dau, H. (2006) Rapid Loss of Structural Motifs in the Manganese Complex of Oxygenic Photosynthesis by X-ray Irradiation at 10-300 K, *J. Biol. Chem. 281*, 4580-4588.

19. Yano, J., Kern, J., Sauer, K., Latimer, M. J., Pushkar, Y., Biesiadka, J., Loll, B., Saenger, W., Messinger, J., Zouni, A., and Yachandra, V. K. (2006) Where Water is Oxidized to Dioxygen: Structure of the Photosynthetic Mn_4Ca Cluster, *Science 314*, 821-825.

20. Debus, R. J. (2008) Protein Ligation of the Photosynthetic Oxygen-Evolving Center, *Coord. Chem. Rev. 252*, 244-258.

21. Dau, H. and Haumann, M. (2007) Time Resolved X-ray Spectroscopy Leads to an Extension of the Classical S-State Cycle Model of Photosynthetic Oxygen Evolution, *Photosynth. Res. 92*, 327-343.

22. Sproviero, E. M., Gascón, J. A., McEvoy, J. P., Brudvig, G. W., and Batista, V. S. (2008) Computation Studies of the O_2-Evolving Complex of Photosystem II and Biomimetic Oxomanganese Complexes, *Coord. Chem. Rev. 252*, 395-415.

23. Wydrzynski, T., Hillier, W., and Messinger, J. (1996) On the Functional Significance of Substrate Accessibility in the Photosynthetic Water Oxidation Mechanism, *Physiol. Plant. 96*, 342-350.

24. Anderson, J. M. (2001) Does Functional Photosystem II Complex have an Oxygen Channel?, *FEBS Lett. 488*, 1-4.

25. Bricker, T. M. and Frankel, L. K. (2002) The structure and function of CP47 and CP43 in Photosystem II, *Photosynth. Res. 72*, 131-146.

26. Rosenberg, C., Christian, J., Bricker, T. M., and Putnam-Evans, C. (1999) Site-directed mutagenesis of glutamate residues in the large extrinsic loop of the photosystem II protein CP 43 affects oxygen-evolving activity and PSII assembly, *Biochemistry 38*, 15994-16000.

27. Strickler, M. A., Hwang, H. J., Burnap, R. L., Yano, J., Walker, L. M., Service, R. J., Britt, R. D., Hillier, W., and Debus, R. J. (2008) Glutamate-354 of the CP43 Polypeptide Interacts with the Oxygen-Evolving Mn_4Ca Cluster of Photosystem II: A Preliminary Characterization of the Glu354Gln Mutant, *Phil. Trans. R. Soc. London, Ser. B 363*, 1179-1188.

28. Shimada, Y., Suzuki, H., Tsuchiya, T., Tomo, T., Noguchi, T., and Mimuro, M. (2009) Effect of a Single-Amino Acid Substitution of the 43 kDa Chlorophyll Protein on the Oxygen-Evolving Reaction of the Cyanobacterium *Synechocystis* sp. PCC 6803: Analysis of the Glu354Gln Mutation., *Biochemistry 48*, 6095-6103.

29. Goldfarb, N., Knoepfle, N., and Putnam-Evans, C. (1997) Contruction of a *psbC* Deletion Strain in *Synechocystis* 6803, *SAAS Bull. Biochem. Biotechnol. 10*, 1-6.

30. Debus, R. J., Campbell, K. A., Gregor, W., Li, Z.-L., Burnap, R. L., and Britt, R. D. (2001) Does Histidine 332 of the D1 Polypeptide Ligate the Manganese Cluster in Photosystem II? An Electron Spin Echo Envelope Modulation Study, *Biochemistry 40*, 3690-3699.

31. Strickler, M. A., Walker, L. M., Hillier, W., Britt, R. D., and Debus, R. J. (2007) No Evidence from FTIR Difference Spectroscopy That Aspartate-342 of the D1 Polypeptide

Ligates a Mn Ion That Undergoes Oxidation during the S_0 to S_1, S_1 to S_2, or S_2 to S_3 Transitions in Photosystem II, *Biochemistry 46*, 3151-3160.

32. Yamanari, T., Kimura, Y., Mizusawa, N., Ishii, A., and Ono, T.-A. (2004) Mid- to Low-Frequency Fourier Transform Infrared Spectra of S-State Cycle for Photosynthetic Water Oxidation in *Synechocystis* sp. PCC 6803, *Biochemistry 43*, 7479-7490.

33. Chu, H.-A., Hillier, W., and Debus, R. J. (2004) Evidence that the C-Terminus of the D1 Polypeptide is Ligated to the Manganese Ion that Undergoes Oxidation During the S_1 to S_2 Transition: An Isotope-Edited FTIR Study, *Biochemistry 43*, 3152-3166.

34. Strickler, M. A., Walker, L. M., Hillier, W., and Debus, R. J. (2005) Evidence from Biosynthetically Incorporated Strontium and FTIR Difference Spectroscopy that the C-Terminus of the D1 Polypeptide of Photosystem II Does Not Ligate Calcium, *Biochemistry 44*, 8571-8577.

35. Chu, H.-A., Nguyen, A. P., and Debus, R. J. (1994) Site-Directed Photosystem II Mutants with Perturbed Oxygen Evolving Properties: 1. Instability or Inefficient Assembly of the Manganese Cluster *In Vivo*, *Biochemistry 33*, 6137-6149.

36. Tang, X.-S. and Diner, B. A. (1994) Biochemical and Spectroscopic Characterization of a New Oxygen-Evolving Photosystem II Core Complex from the Cyanobacterium *Synechocystis* sp. PCC 6803, *Biochemistry 33*, 4594-4603.

37. Burnap, R. L., Qian, M., and Pierce, C. (1996) The Manganese-Stabilizing Protein of Photosystem II Modifies the *in vivo* Deactivation Kinetics of the H_2O Oxidation Complex in *Synechocystis* sp. PCC 6803, *Biochemistry 35*, 874-882.

38. Qian, M., Dao, L., Debus, R. J., and Burnap, R. L. (1999) Impact of Mutations within the Putative Ca^{2+}-Binding Lumenal Interhelical a-b Loop of the Photosystem II D1 Protein

on the Kinetics of Photoactivation and H_2O-Oxidation in *Synechocystis* sp. PCC 6803, *Biochemistry 38*, 6070-6081.

39. Lavorel, J. (1976) Matrix Analysis of the Oxygen Evolving System of Photosynthesis, *J. Theor. Biol. 57*, 171-185.

40. Meunier, P. C., Burnap, R. L., and Sherman, L. A. (1996) Improved 5-step Modeling of the Photosystem II S-state Mechanism in Cyanobacteria, *Photosynth. Res. 47*, 61-76.

41. Jursinic, P. A. and Dennenberg, R. J. (1990) Oxygen Release Time in Leaf Discs and Thylakoids of Peas and Photosystem II Membrane Fragments of Spinach, *Biochim. Biophys. Acta 1020*, 195-206.

42. Debus, R. J., Aznar, C., Campbell, K. A., Gregor, W., Diner, B. A., and Britt, R. D. (2003) Does Aspartate 170 of the D1 Polypeptide Ligate the Manganese Cluster in Photosystem II? An EPR and ESEEM Study, *Biochemistry 42*, 10600-10608.

43. Yano, J., Pushkar, Y., Glatzel, P., Lewis, A., Sauer, K., Messinger, J., Bergmann, U., and Yachandra, V. K. (2005) High-Resolution Mn EXAFS of the Oxygen-Evovling Complex in Photosystem II: Structural Implications for the Mn_4Ca Cluster, *J. Am. Chem. Soc.* 14974-14975.

44. Debus, R. J., Strickler, M. A., Walker, L. M., and Hillier, W. (2005) No Evidence from FTIR Difference Spectroscopy That Aspartate-170 of the D1 Polypeptide Ligates a Manganese Ion That Undergoes Oxidation during the S_0 to S_1, S_1 to S_2, or S_2 to S_3 Transitions in Photosystem II, *Biochemistry 44*, 1367-1374.

45. Strickler, M. A., Hillier, W., and Debus, R. J. (2006) No Evidence from FTIR Difference Spectroscopy that Glutamate-189 of the D1 Polypeptide Ligates a Mn Ion that Undergoes

Oxidation During the S_0 to S_1, S_1 to S_2, or S_2 to S_3 Transitions in Photosystem II, *Biochemistry 45*, 8801-8811.

46. Noguchi, T. and Sugiura, M. (2002) Flash-Induced FTIR Difference Spectra of the Water Oxidizing Complex in Moderately Hydrated Photosystem II Core Films: Effect of Hydration Extent on S-State Transitions, *Biochemistry 41*, 2322-2330.

47. Service, R. J., Hillier, W., and Debus, R. J. (2010) Evidence from FTIR Difference Spectroscopy of an Extensive Network of Hydrogen Bonds near the Oxygen-Evolving Mn_4Ca Cluster of PhotosystemII Involving D1-Glu65, D2-Glu312, and D1-Glu329, *Biochemistry 49*, 6655-6669.

48. Robblee, J. H., Messinger, J., Cinco, R. M., McFarlane, K. L., Fernandez, C., Pizarro, S. A., Sauer, K., and Yachandra, V. K. (2002) The Mn Cluster in the S0 State of the Oxygen-Evolving Complex of Photosystem II Studied by EXAFS Spectroscopy: Are There Three Di-μ-oxo-bridged Mn_2 Moieties in the Tetranuclear Mn Complex?, *J. Am. Chem. Soc. 124*, 7459-7471.

49. Singh, S., Debus, R. J., Wydrzynski, T., and Hillier, W. (2008) Investigation of Substrate Water Interactions at the High-Affinity Mn Site in the Photosystem II Oxygen-Evolving Complex, *Phil. Trans. R. Soc. London, Ser. B 363*, 1229-1235.

50. Hillier, W. and Wydrzynski, T. (2004) Substrate Water Interactions within the Photosystem II Oxygen Evolving Complex, *Phys. Chem. Chem. Phys. 6*, 4882-4889.

51. Gilchrist, M. L., Jr., Ball, J. A., Randall, D. W., and Britt, R. D. (1995) Proximity of the Manganese Cluster of Photosystem II to the Redox Active Tyrosine Y_Z, *Proc. Natl. Acad. Sci. USA 92*, 9545-9549.

52. Peloquin, J. M., Campbell, K. A., and Britt, R. D. (1998) ^{55}Mn Pulsed ENDOR Demonstrates that the Photosystem II "Split" EPR Signal Arises from a Magnetically-Coupled Mangano-Tyrosyl Complex, *J. Am. Chem. Soc. 120*, 6840-6841.

53. Lakshmi, K. V., Eaton, S. S., Eaton, G. R., Frank, H. A., and Brudvig, G. W. (1998) Analysis of Dipolar and Exchange Interactions between Manganese and Tyrosine Z in the S2YZdot State of Acetate-Inhibited Photosystem II via EPR Spectral Simulations at X- and Q- bands, *J. Phys. Chem. B 102*, 8327-8335.

54. Dorlet, P., Boussac, A., Rutherford, A. W., and Un, S. (1999) Multifrequency High-Field EPR Study of the Interaction between the Tyrosyl Z Radical and the Manganese Cluster in Plant Photosystem II, *J. Phys. Chem. B 103*, 10945-10954.

55. Chu, H.-A., Hillier, W., Law, N. A., and Babcock, G. T. (2001) Vibrational Spectroscopy of the Oxygen-Evolving Complex and of Manganese Model Compounds, *Biochim. Biophys. Acta 1503*, 69-82.

56. Noguchi, T. and Berthomieu, C. (2005) Molecular Analysis by Vibrational Spectroscopy, in *Photosystem II: The Light-Driven Water:Plastoquinone Oxidoreductase* (Wydrzynski, T. and Satoh, Ki., Eds.) pp 367-387, Springer, Dordrecht, The Netherlands.

57. Noguchi, T. (2007) Light-Induced FTIR Difference Spectroscopy as a Powerful Tool Toward Understanding the Molecular Mechanism of Photosynthetic Oxygen Evolution, *Photosyn. Res. 91*, 59-69.

58. Noguchi, T. (2008) Fourier Transform Infrared Analysis of the Photosynthetic Oxygen-Evolving Center, *Coord. Chem. Rev. 251*, 336-346.

59. Hienerwadel, R., Boussac, A., Breton, J., Diner, B. A., and Berthomieu, C. (1997) Fourier Transform Infrared Difference Spectroscopy of Photosystem II Tyrosine D using Site-Directed Mutagenesis and Specific Isotope Labeling, *Biochemistry 36*, 14712-14723.

60. Noguchi, T., Inoue, Y., and Tang, X. S. (1997) Structural coupling between the oxygen-evolving Mn cluster and a tyrosine residue in photosystem II as revealed by Fourier transform infrared spectroscopy, *Biochemistry 36*, 14705-14711.

61. Berthomieu, C., Hienerwadel, R., Boussac, A., Breton, J., and Diner, B. A. (1998) Hydrogen-Bonding of Redox-Active Tyrosine Z of Photosystem II Probed by FTIR Difference Spectroscopy, *Biochemistry 37*, 10547-10554.

62. Chu, H.-A., Debus, R. J., and Babcock, G. T. (2001) D1-Asp170 is Structurally Coupled to the Oxygen Evolving Complex in Photosystem II as Revealed by Light-Induced Fourier Transform Infrared Difference Spectroscopy, *Biochemistry 40*, 2312-2316.

63. Kimura, Y., Mizusawa, N., Ishii, A., Nakazawa, S., and Ono, T.-A. (2005) Changes in Structural and Functional Properties of Oxygen-Evolving Complex Induced by Replacement of D1-Glutamate 189 with Glutamine in Photosystem II: Ligation of Glutamate 189 Carboxylate to the Manganese Cluster, *J. Biol. Chem. 280*, 37895-37900.

64. Mizusawa, N., Kimura, Y., Ishii, A., Yamanari, T., Nakazawa, S., Teramoto, H., and Ono, T.-A. (2004) Impact of Replacement of D1 C-terminal Alanine with Glycine on Structure and Function of Photosynthetic Oxygen-Evolving Complex, *J. Biol. Chem. 279*, 29622-29627.

65. Mizusawa, N., Yamanari, T., Kimura, Y., Ishii, A., Nakazawa, S., and Ono, T.-A. (2004) Changes in the Functional and Structural Properties of the Mn Cluster Induced by

Replacing the Side Group of the C-Terminus of the D1 Protein of Photosystem II, *Biochemistry 43*, 14644-14652.

66. Kimura, Y., Mizusawa, N., Yamanari, T., Ishii, A., and Ono, T.-A. (2005) Structural Changes of D1 C-terminal α-Carboxylate during S-state Cycling of Photosynthetic Oxygen Evolution, *J. Biol. Chem. 280*, 2078-2083.

67. Noguchi, T., Ono, T.-A., and Inoue, Y. (1995) Direct Detection of a Carboxylate Bridge Between Mn and Ca^{2+} in the Photosynthetic Oxygen-Evolving Center by Means of Fourier Transform Infrared Spectroscopy, *Biochim. Biophys. Acta 1228*, 189-200.

68. Noguchi, T. and Sugiura, M. (2003) Analysis of Flash-Induced FTIR Difference Spectra of the S-State Cycle in the Photosynthetic Water-Oxidizing Complex by Uniform ^{15}N and ^{13}C Isotope Labeling, *Biochemistry 42*, 6035-6042.

69. Kimura, Y., Mizusawa, N., Ishii, A., Yamanari, T., and Ono, T.-A. (2003) Changes of Low-Frequency Vibrational Modes Induced by Universal ^{15}N- and ^{13}C-Isotope Labeling in S_2/S_1 FTIR Difference Spectrum of Oxygen-Evolving Complex, *Biochemistry 42*, 13170-13177.

70. Noguchi, T., Sugiura, M., and Inoue, Y. (1999) FTIR Studies on the Amino-Acid Ligands of the Photosynthetic Oxygen-Evolving Mn-Cluster, in *Fourier Transform Spectroscopy: Twelfth International Conference* (Itoh, K. and Tasumi, M., Eds.) pp 459-460, Waseda University Press, Tokyo, Japan.

71. Messinger, J., Badger, M., and Wydrzynski, T. (1995) Detection of *one* Slowly Exchanging Substrate Water Molecule in the S_3 state of Photosystem II, *Proc. Natl. Acad. Sci. USA 92*, 3209-3213.

72. Hillier, W., Messinger, J., and Wydrzynski, T. (1998) Kinetic Determination of the Fast Exchanging Substrate Water Molecule in the S_3 State of Photosystem II, *Biochemistry 37*, 16908-16914.

73. Hillier, W., Hendry, G., Burnap, R. L., and Wydrzynski, T. (2001) Substrate Water Exchange in Photosystem II Depends on the Peripheral Proteins, *J. Biol. Chem. 276*, 46917-46924.

74. Konermann, L., Messinger, J., and Hillier, W. (2008) Mass Spectrometry-Based Methods for Studying Kinetics and Dynamics in Biological Systems, in *Biophysical Techniques in Photosynthesis II* (Aartsma, T. J. and Matysik, J., Eds.) pp 167-190, Springer, Dordrecht, The Netherlands.

75. Hillier, W. and Wydrzynski, T. (2008) ^{18}O-Water Exchange in Photosystem II: Substrate Binding and Intermediates of the Water Splitting Cycle, *Coord. Chem. Rev. 252*, 306-317.

76. McEvoy, J. P. and Brudvig, G. W. (2004) Structure-Based Mechanism of Photosynthetic Water Oxidation, *Phys. Chem. Chem. Phys. 6*, 4754-4763.

77. Haumann, M., Liebisch, P., Müller, C., Barra, M., Grabolle, M., and Dau, H. (2005) Photosynthetic O_2 Formation Tracked by Time-Resolved X-ray Experiments, *Science 310*, 1019-1021.

78. Sproviero, E. M., Gascón, J. A., McEvoy, J. P., Brudvig, G. W., and Batista, V. S. (2008) Quantum Mechanics/Molecular Mechanics Study of the Catalytic Cycle of Water Splitting In Photosystem II, *J. Am. Chem. Soc. 130*, 3428-3442.

79. Sproviero, E. M., McEvoy, J. P., Gascón, J. A., Brudvig, G. W., and Batista, V. S. (2008) Computational Insights into the O2-Evolving Complex of Photosystem II, *Photosynth. Res. 97*, 91-114.

80. Tommos, C. and Babcock, G. T. (2000) Proton and Hydrogen Currents in Photosynthetic Water Oxidation, *Biochim. Biophys. Acta 1458*, 199-219.

81. Ishikita, H., Saenger, W., Loll, B., Biesiadka, J., and Knapp, E.-W. (2006) Energetics of a Possible Proton Exit Pathway for Water Oxidation in Photosystem II, *Biochemistry 45*, 2063-2071.

82. Murray, J. W. and Barber, J. (2007) Structural Characteristics of Channels and Pathways in Photosystem II Including the Identification of an Oxygen Channel, *J. Struct. Biol. 159*, 228-237.

83. Ho, F. M. and Styring, S. (2008) Access Channels and Methanol Binding Site to the $CaMn_4$ Cluster in Photosystem II based on Solvent Accessibility Simulation, with Implications for Substrate Water Access, *Biochim. Biophys. Acta 1777*, 140-153.

84. Gabdulkhakov, A., Guskov, A., Broser, M., Kern, J., Müh, F., Saenger, W., and Zouni, A. (2009) Probing the Accessibility of the Mn_4Ca Cluster in Photosystem II: Channels Calculation, Noble Gas Derivatization, and Cocrystallization with DMSO, *Structure 17*, 1223-1234.

85. Wraight, C. A. (2006) Chance and Design - Proton Transfer in Water, Channels and Bioenergetic Proteins, *Biochim. Biophys. Acta 1757*, 886-912.

86. Silverman, D. N. and McKenna, R. (2007) Solvent-Mediated Proton Transfer in Catalysis by Carbonic Anhydrase, *Acc. Chem. Res. 40*, 669-675.

87. Mikulski, R. L. and Silverman, D. N. (2010) Proton Transfer in Catalysis and the Role of Proton Shuttles in Carbonic Anhydrase, *Biochim. Biophys. Acta 1804*, 422-426.

88. Okamura, M. Y., Paddock, M. L., Graige, M. S., and Feher, G. (2000) Proton and electron transfer in bacterial reaction centers, *Biochim. Biophys. Acta 1458*, 148-163.

89. Paddock, M. L., Feher, G., and Okamura, M. Y. (2003) Proton Transfer Pathways and Mechanism in Bacterial Reaction Centers, *FEBS Lett. 555*, 45-50.

90. Wraight, C. A. (2005) Intraprotein Proton Transfer - Concepts and Realities from the Bacterial Photosynthetic Reaction Center, in *Biophysical and Structural Aspects of Bioenergetics* (Wikström, M., Ed.) pp 273-313, RSC Publishing, Cambridge, UK.

91. Hosler, J. P., Ferguson-Miller, S., and Mills, D. A. (2006) Energy Transduction: Proton Transfer Through the Respiratory Complexes, *Annu. Rev. Biochem. 75*, 165-187.

92. Wikström, M. and Verkhovsky, M. I. (2007) Mechanism and Energetics of Proton Translocation by the Respiratory Heme-Copper Oxidases, *Biochim. Biophys. Acta 1767*, 1200-1214.

93. Brzezinski, P. and Gennis, R. B. (2008) Cytochrome *c* Oxidase: Exciting Progress and Remaining Mysteries, *J. Bioenerg. Biomemb. 40*, 521-531.

94. Boussac, A., Zimmermann, J.-L., and Rutherford, A. W. (1989) EPR Signals from Modified Charge Accumulation States of the Oxygen Evolving Enzyme in Ca^{2+}-Deficient Photosystem II, *Biochemistry 28*, 8984-8989.

95. Sivaraja, M., Tso, J., and Dismukes, G. C. (1989) A Calcium-Specific Site Influences the Structure and Activity of the Manganese Cluster Responsible for Photosynthetic Water Oxidation, *Biochemistry 28*, 9459-9464.

96. Ono, T.-A. and Inoue, Y. (1989) Removal of Ca by pH 3.0 Treatment Inhibits S_2 to S_3 Transition in Photosynthetic Oxygen Evolution System, *Biochim. Biophys. Acta 973*, 443-449.

97. Boussac, A., Zimmermann, J.-L., and Rutherford, A. W. (1990) Factors Influencing the Formation of Modified S_2 EPR Signal and the S_3 EPR Signal in Ca^{2+}-Depleted Photosystem II, *FEBS Lett. 277*, 69-74.

98. Haumann, M. and Junge, W. (1999) Evidence for Impaired Hydrogen-Bonding of Tyrosine Y_Z in Calcium-Depleted Photosystem II, *Biochim. Biophys. Acta 1411*, 121-133.

99. Styring, S., Feyziyev, Y., Mamedov, F., Hillier, W., and Babcock, G. T. (2003) pH Dependence of the Donor Side Reactions in Ca^{2+}-Depleted Photosystem II, *Biochemistry 42*, 6185-6192.

100. Burnap, R. L. (2004) D1 Protein Processing and Mn Cluster Assembly in Light of the Emerging Photosystem II Structure, *Phys. Chem. Chem. Phys. 6*, 4803-4809.

101. DasGupta, J., Ananyev, G., and Dismukes, G. C. (2008) Photoassembly of the Water-Oxidizing Complex in Photosystem II, *Coord. Chem. Rev. 252*, 347-360.

102. Yano, J., Walker, L. M., Yachandra, V. K., and Debus, R. J. (2010) Altered Structure of the Mn_4Ca Cluster in the Oxygen Evolving Complex of Photosystem II in a Cyanobacteria Mutant (*submitted*).

103. Peloquin, J. M., Campbell, K. A., Randall, D. W., Evanchik, M. A., Pecoraro, V. L., Armstrong, W. H., and Britt, R. D. (2000) ^{55}Mn ENDOR of the S_2-state Multiline EPR Signal of Photosystem II: Implications on the Structure of the Tetranuclear Mn Cluster, *J. Am. Chem. Soc. 122*, 10926-10942.

104. Kulik, L., Epel, B., Lubitz, W., and Messinger, J. (2005) ^{55}Mn Pulse ENDOR at 34 GHz of the S_0 and S_2 States of the Oxygen-Evolving Complex in Photosystem II, *J. Am. Chem. Soc. 127*, 2392-2393.

105. Kulik, L., Epel, B., Lubitz, W., and Messinger, J. (2007) Electronic Structure of the Mn_4O_xCa Cluster in the S_0 and S_2 States of the Oxygen-Evolving Complex of Photosystem II Based on Pulse ^{55}Mn-ENDOR and EPR Spectroscopy, *J. Am. Chem. Soc. 129*, 13421-13435.

106. Debus, R. J., Campbell, K. A., Peloquin, J. M., Pham, D. P., and Britt, R. D. (2000) Histidine 332 of the D1 Polypeptide Modulates the Magnetic and Redox Properties of the Manganese Cluster and Tyrosine Y_Z in Photosystem II, *Biochemistry 39*, 470-478.

107. Boussac, A., Rappaport, F., Carrier, P., Verbavatz, J.-M., Gobin, R., Kirilovsky, D., Rutherford, A. W., and Sugiura, M. (2004) Biosynthetic Ca^{2+}/Sr^{2+} Exchange in the Photosystem II Oxygen-Evolving Enzyme of *Thermosynechococcus elongatus*, *J. Biol. Chem. 279*, 22809-22819.

108. Mehrotra, R. C. and Bohra, R. (1983) *Metal Carboxylates* Academic Press, London, UK.

109. Deacon, G. B. and Phillips, R. J. (1980) Relationships between the Carbon-Oxygen Stretching Frequencies of Carboxylato Complexes and the Type of Carboxylate Coordination, *Coord. Chem. Rev. 33*, 227-250.

110. Tackett, J. E. (1989) FT-IR Characterization of Metal Acetates in Aqueous Solution, *Appl. Spectrosc. 43*, 483-489.

111. Nakamoto, K. (1997) Infrared and Raman Spectra of Inorganic and Coordination Compounds, Part B: Applications in Coordination, Organometallic, and Bioinorganic Chemistry, 5th ed., John Wiley & Sons, New York, NY.

112. Nara, M., Torii, H., and Tasumi, M. (1996) Correlation between the Vibrational Frequencies of the Carboxylate Group and Types of its Coordination to a Metal Ion: An *ab Initio* Molecular Orbital Study, *J. Phys. Chem. 100*, 19812-19817.

113. Venyaminov, S. Yu. and Kalnin, N. N. (1990) Quantitative IR Spectrophotometry of Peptide Compounds in Water (H_2O) Solutions. 1. Spectral Parameters of Amino Acid Residue Absorption Bands, *Biopolymers 30*, 1243-1257.

114. Rahmelow, K., Hübner, W., and Ackermann, Th. (1998) Infrared Absorbances of Protein Side Chains, *Anal. Biochem. 257*, 1-11.

115. Barth, A. (2000) The Infrared Absorption of Amino Acid Side Chains, *Prog. Biophys. Molec. Biol. 74*, 141-173.

116. Barth, A. and Zscherp, C. (2002) What Vibrations Tell Us About Proteins, *Q. Rev. Biophys. 35*, 369-430.

117. Hillier, W. and Wydrzynski, T. (2001) Oxygen Ligand Exchange at Metal sites - Implications for the O_2 Evolving Mechanism of Photosystem II, *Biochim. Biophys. Acta 1503*, 197-209.

118. Vassiliev, S., Comte, P., Mahboob, A., and Bruce, D. (2010) Tracking the Flow of Water through Photosystem II Using Molecular Dynamics and Streamline Tracing, *Biochemistry 49*, 1873-1881.

119. Richens, D. T. (2005) Ligand Substitution Reactions at Inorganic Centers, *Chem. Rev. 105*, 1961-2002.

120. Hendry, G. and Wydrzynski, T. (2002) The Two Substrate-Water molecules are Already Bound to the Oxygen-Evolving Complex in the S_2 State of Photosystem II, *Biochemistry 41*, 13328-13334.

121. Noguchi, T. and Sugiura, M. (2000) Structure of an Active Water Molecule in the Water-Oxidizing Complex of Photosystem II As Studied by FTIR Spectroscopy, *Biochemistry 39*, 10943-10949.

122. Noguchi, T. and Sugiura, M. (2002) FTIR Detection of Water Reactions During the Flash-Induced S-State Cycle of the Photosynthetic Water-Oxidizing Complex, *Biochemistry 41*, 15706-15712.

123. Suzuki, H., Sugiura, M., and Noguchi, T. (2008) Monitoring Water Reactions during the S-State Cycle of the Photosynthetic Water-Oxidizing Center: Detection of the DOD Bending Vibrations by Means of Fourier Transform Infrared Spectroscopy, *Biochemistry 47*, 11024-11030.

124. Su, J.-H., Lubitz, W., and Messinger, J. (2008) Probing Mode and Site of Substrate Water Binding to the Oxygen-Evolving Complex in the S_2 State of Photosystem II by ^{17}O-HYSCORE Spectroscopy, *J. Am. Chem. Soc. 130*, 786-787.

125. Su, J.-H. and Messinger, J. (2010) Is Mn-Bound Substrate Water Protonated in the S_2 State of Photosystem II?, *Appl. Magn. Reson. 37*, 123-136.

Table 1. S-state decay cycling parameters of CP43-E354Q membranes [a]

Strain	S-state distribution: S_0:S_1:S_2:S_3 (%)	Misses α (%)	Hits β (%)	Double hits γ (%)	Deactivations δ (%)
Wild-Type	36:62:2:0	9	86	3	2
CP43-E354Q	31:63:6:0	9	84	4	3

[a] Membranes were given a series of 20 pre-flashes followed by a 10 min dark-adaptation period prior to the initiation of the measuring flash sequence. Numerical analysis of the O_2 flash-yield amplitudes was performed assuming a four-state model as described previously (*39, 40*).

Table 2: Rate constants for ^{18}O exchange in the S_3 state of Wild-type and CP43-E354Q thylakoid membranes from *Synechocystis* sp. PCC 6803 [a]

Sample	k_1 (s^{-1})	k_2 (s^{-1})
WT	0.47±0.04	19.7±1.3
CP43-E354Q	0.86±0.35	167±38

[a] Buffer solution medium: 40 mM MES, pH 6.5, 15 mM $MgCl_2$, 15 mM $CaCl_2$, 10% glycerol, 1.2 M betaine

FIGURE LEGENDS

FIGURE 1. Comparison of the flash O_2 yield patterns of wild-type (A) and CP43-E354Q (B) thylakoid membranes in response to 15 saturating xenon flashes applied at a frequency of 4 Hz. Equivalent amounts of thylakoid membranes were deposited centrifugally on the surface of a bare-platinum electron, subjected to 20 preflashes, then dark-adapted for ten minutes before the sequence of measuring flashes was initiated.

FIGURE 2. Comparison of the flash-induced O_2 signals of wild-type (black traces) and CP43-E354Q (red traces) thylakoid membranes plotted on (A) linear and (B) logarithmic time scales. The traces have been normalized to facilitate comparison (the data of the mutant was multiplied vertically by a factor of 3.6). Equivalent amounts of thylakoid membranes were deposited centrifugally on the surface of a bare-platinum electrode and given a sequence of 100 saturating xenon flashes at 4 Hz. The data show the averages from each set of 100 kinetic traces.

FIGURE 3. Comparison of the parallel polarization S_1 state (A) and light-*minus*-dark perpendicular polarization S_2 state (B) multiline EPR signals of wild-type (black) and CP43-E354Q (red) PSII core complexes. The wild-type and mutant samples in (A) contained 125 μL of 6.7 mg of Chl/mL and 8.1 mg of Chl/mL, respectively and were deaerated prior to measurement to remove condensed O_2. To facilitate comparison, the mutant spectrum has been multiplied vertically by a factor of 4. Features below 375 G or above 650 G in the mutant spectrum were not reproducible. The sample buffer in (A) consisted of 1.2 M betaine, 10% (v/v) glycerol, 10 mM MES-NaOH (pH 6.0), 10 mM $CaCl_2$, 5 mM $MgCl_2$, 50 mM histidine, 1 mM

EDTA, and 0.03% (w/v) *n*-dodecyl β-D-maltoside. The wild-type and mutant samples in (B) contained 100 μL of 11.0 mg of Chl/mL and 60 μL of 10.9 mg of Chl/mL, respectively. The sample buffer consisted of 1.2 M betaine, 40% (v/v) glycerol, 10 mM MES-NaOH (pH 6.0), 10 mM $CaCl_2$, 5 mM $MgCl_2$, and 0.03% (w/v) *n*-dodecyl β-D-maltoside. The data in (A) were recorded at 4.7 K with a microwave frequency of 9.3822 GHz, a microwave power of 50 mW, a modulation amplitude of 9 G, a modulation frequency of 100 GHz, a time constant of 81 ms, and a scan time of 170 s/1100 G. The wild-type and mutant spectra represent the averages of 25 and 100 scans, respectively. The data in (B) were recorded at 9 K with a microwave frequency of 9.2579 GHz, a microwave power of 5 mW, a modulation amplitude of 8 G, a modulation frequency of 100 kHz, a time constant of 250 ms, and a scan time of 4 min/3300 G. To generate the S_2 state in (B), samples were illuminated for 5 min at 195 K before being flash-frozen in liquid nitrogen. Both spectra in (B) have had the large signal of $Y_D^{\bullet}$ at $g = 2$ excised for clarity. Each spectrum in (B) represents the average of 60 scans. To correct for the lower amount of Chl in the mutant sample, the mutant spectrum in (B) has been multiplied vertically by a factor of 1.67. Asterisks denote peaks used to estimate the relative amplitudes of the signals (see text). The insert in (B) shows light-*minus*-dark scans between 600 and 3800 G.

FIGURE 4. The decay of the S_2 state in CP43-E354Q PSII core complexes as measured from the decay of the S_2 state multiline EPR signal at 4°C. The signal amplitude was estimated from the area under the six low-field lines shown as asterisks in Figure 3.

FIGURE 5. Comparison of the Mn K-edge XANES spectra of wild-type (blue traces) and CP43-E354Q (red traces) in PSII core complexes poised in the S_1 state by extensive dark-adaptation

(A) and in the S_2 state after illumination (B). The corresponding second derivatives of the data in (A) and (B) are shown in (C) and (D), respectively.

FIGURE 6. Comparison of the Fourier transforms of k^3-weighted Mn-EXAFS of wild-type (A) and CP43-E354Q (B) PSII core complexes poised in the S_1 (blue traces) and S_2 traces (red traces). The wild-type spectra from (A) are reproduced in (B) in grey.

FIGURE 7. Comparison of the mid-frequency FTIR difference spectra of wild-type (black traces) and CP43-E354Q (red traces) PSII core complexes in response to four successive flash illuminations applied at 273 K and spaced by 96 s. The spectra were normalized to the peak-to-peak amplitudes of the negative ferricyanide peak at 2115 cm^{-1} and the positive ferrocyanide peak at 2038 cm^{-1} (these peaks reflect the reduction of the ferricyanide electron acceptor by $Q_A^{\bullet-}$). The wild-type spectra represent the averages of seven samples (5,600 scans). The CP43-E354Q spectra represent the averages of nine samples (7,200 scans). Samples were given a single set of four flashes at 273 K after having been dark adapted for 18 hours at the same temperature. The data recorded after the 1st flash are dominated by the S_1 to S_2 transition and represent S_2-*minus*-S_1 FTIR difference spectra. Dark-*minus*-dark control spectra are included to show the noise level (lower traces).

FIGURE 8. Comparison of the mid-frequency S_2-*minus*-S_1 FTIR difference spectra of wild-type (black traces) and CP43-E354Q (red traces) PSII core complexes purified and examined under a variety of conditions. In panel (A), samples were purified in the presence of 1.2 M betaine and 10% (v/v) glycerol, dark adapted for 18 hr, then subjected to a single set of flashes at 273 K (data

reproduced from Figure 8, top set of traces). In panel (B), samples were purified in the presence of 25% (v/v) glycerol, dark adapted 2 h, then given a single flash at 250 K [the wild-type and mutant samples correspond to the averages of three samples (2,400 scans) and four samples (3,200 scans), respectively]. In panel (C), samples were purified in the presence of 25% (v/v) glycerol, dark adapted 2 h, then given 16 flashes spaced 30 min apart at 273 K [the wild-type and mutant samples correspond to the averages of four samples each (12,800 scans each). In panel (D), samples were purified in the presence of 1.2 M betaine and 10% (v/v) glycerol, dark adapted 2 h, then given 16 flashes spaced 30 min apart at 273 K [the wild-type and mutant samples correspond to the averages of four samples each (12,800 scans each). Within each panel, the spectra were normalized to the peak-to-peak amplitudes of the negative ferricyanide peak at 2115 cm^{-1} and the positive ferrocyanide peak at 2038 cm^{-1}.

FIGURE 9. Comparison of the mid-frequency S_2-*minus*-S_1 FTIR difference spectra of unlabeled (black traces) and ^{15}N-globally-labeled (blue traces) wild-type (A) and CP43-E354Q (B) PSII core complexes in response to a single flash applied at 273 K. The unlabeled spectra in (A) and (B) are reproduced from Figure 7, top traces (black and red, respectively). The ^{15}N-labeled wild-type and CP43-E354Q spectra represents the averages of nine (7,200 scans) and eight samples (6,400 scans), respectively. Samples were given a single flash at 273 K after having been dark adapted for 18 hours at the same temperature.

FIGURE 10. Comparison of the double difference spectra (wild-type-*minus*-mutant) that were obtained by subtracting the S_2-*minus*-S_1 FTIR difference spectrum of unlabeled or ^{15}N-labeled CP43-E354Q PSII core complexes from the S_2-*minus*-S_1 FTIR difference spectrum of unlabeled

or ^{15}N-labeled wild-type PSII complexes recorded under each of the conditions shown in Figure 9. Double difference spectra obtained by subtracting the spectra of unlabeled samples are shown with black lines. Double difference spectra obtained by subtracting the spectra of ^{15}N-labeled samples are shown with blue lines. The unlabeled double difference spectra in panels (A), (B), (C), and (D) were obtained by directly subtracting the data of Figure 9A, 9B, 9C, and 9D, respectively. The ^{15}N-labeled double difference spectrum in panel (A) was obtained by subtracting the ^{15}N-labeled spectra shown in Figure 8.

FIGURE 11. Comparison of the mid-frequency S_2-*minus*-S_1 FTIR difference spectra of unlabeled (black traces) and L-[1-^{13}C]alanine-labeled (red traces) wild-type (A) or CP43-E354Q (B) PSII core complexes. Each sample was given a single flash at 273 K after having been dark-adapted for 18 hours at the same temperature. The spectra of the unlabeled wild-type and CP43-E354Q PSII core complexes have been normalized to the peak-to-peak amplitudes of the negative ferricyanide peak at 2115 cm^{-1} and the positive ferrocyanide peak at 2038 cm^{-1}. The unlabeled and L-[1-^{13}C]alanine-labeled wild-type spectra in (A) represent the averages of seven samples (5,600 scans) and eight samples (6,400 scans), respectively. The unlabeled and L-[1-^{13}C]alanine-labeled CP43-E354Q spectra in (B) each represent the averages of nine samples (7,200 scans). Within each panel, the spectra have been normalized to maximize their overlap between 1500 and 1350 cm^{-1}. Panel (C) shows the double difference spectra, ^{12}C-*minus*-^{13}C, of wild-type (black trace) and CP43-E354Q (red trace) PSII core complexes that were obtained by subtracting the S_2-*minus*-S_1 FTIR difference spectra of the L-[1-^{13}C]alanine-labeled core complexes from the S_2-*minus*-S_1 FTIR difference spectra of the unlabeled core complexes (the spectra shown in Figures 11A and 11B were subtracted directly). Only the regions between 1380

and 1280 cm^{-1} are shown.

FIGURE 12. ^{18}O exchange measurements in the S_3 state of wild-type (black circles and line) and CP43-E354Q (red circles and line) thylakoid membranes. The data are shown as filled circles with the kinetic fit shown by a line. The inset shows the same data plotted a shorter expanded time scale to show the fast phase of exchange.

Actual Size – Single Column Figure

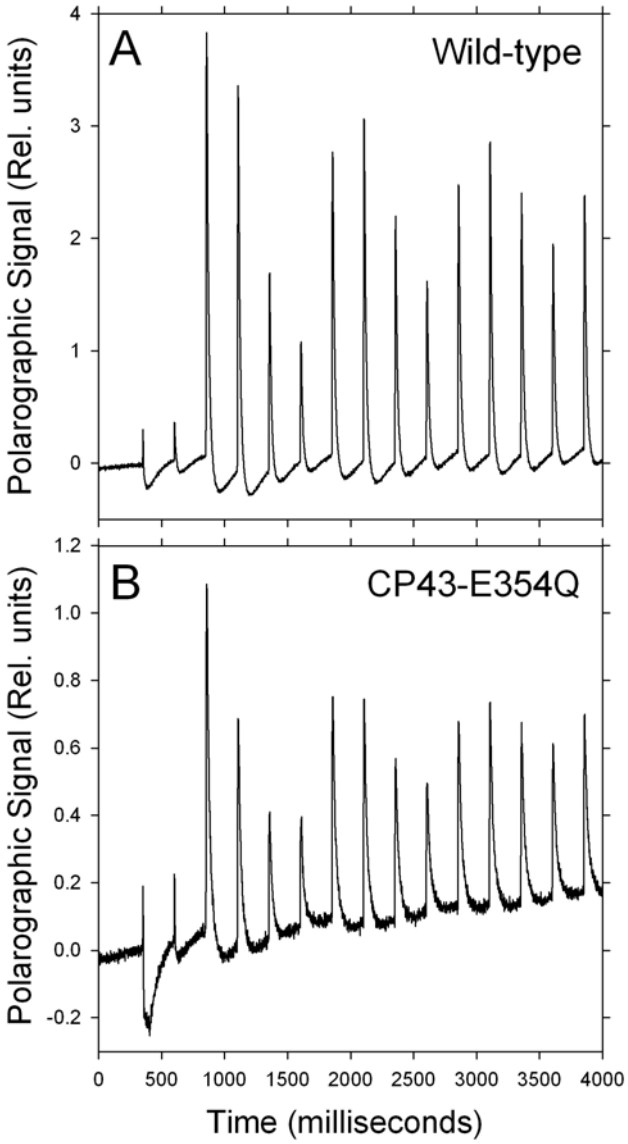

Service et al. **Figure 1**

Actual Size – Single Column Figure

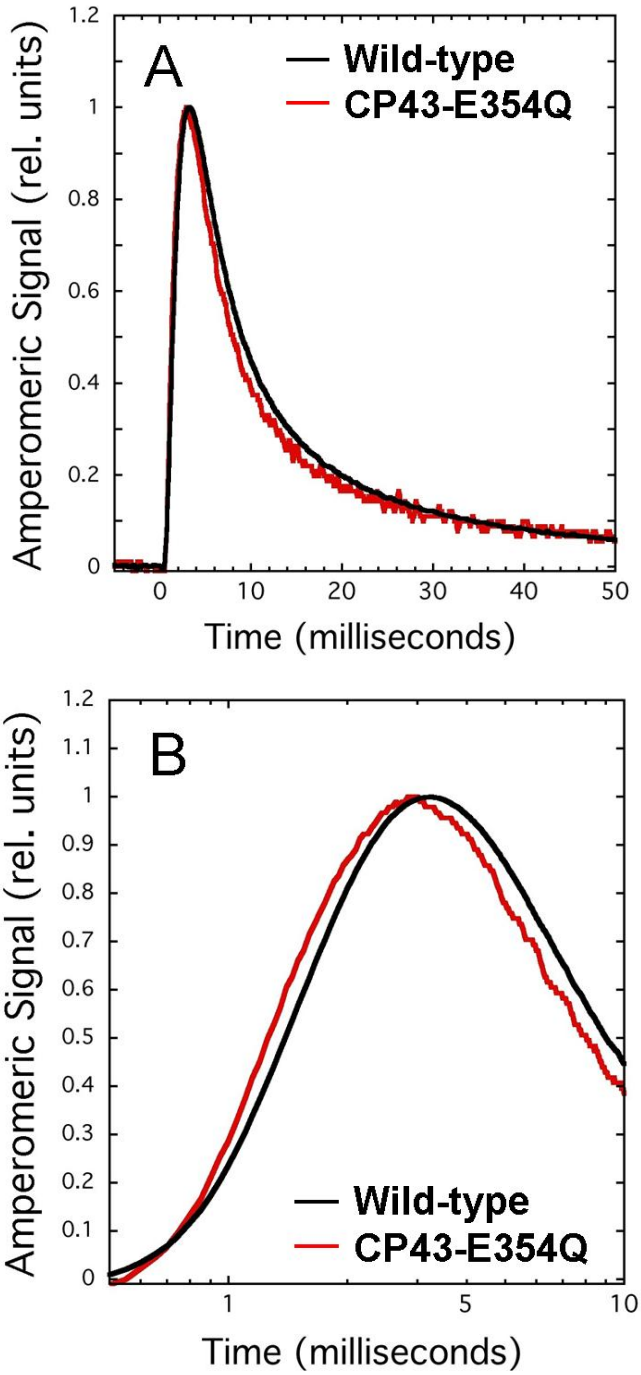

Service et al. **Figure 2**

Actual Size – Single Column Figure

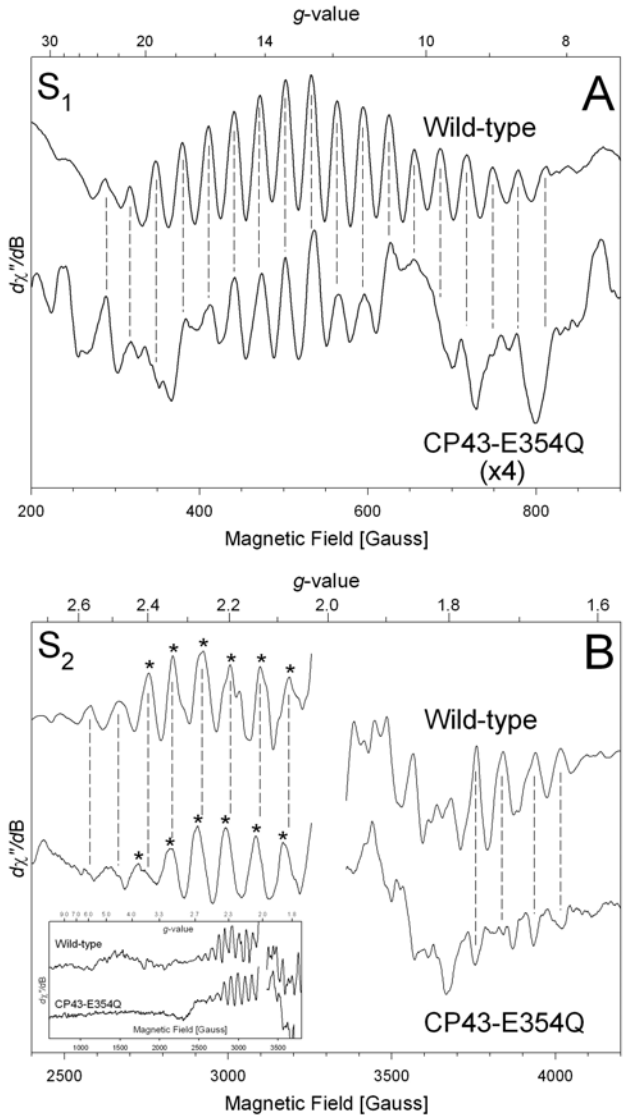

Service et al. **Figure 3**

Actual Size – Single Column Figure

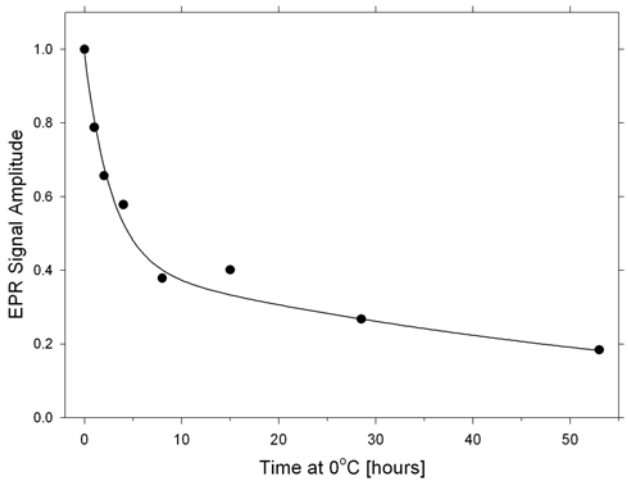

Service et al. **Figure 4**

Actual Size – Double Column Figure

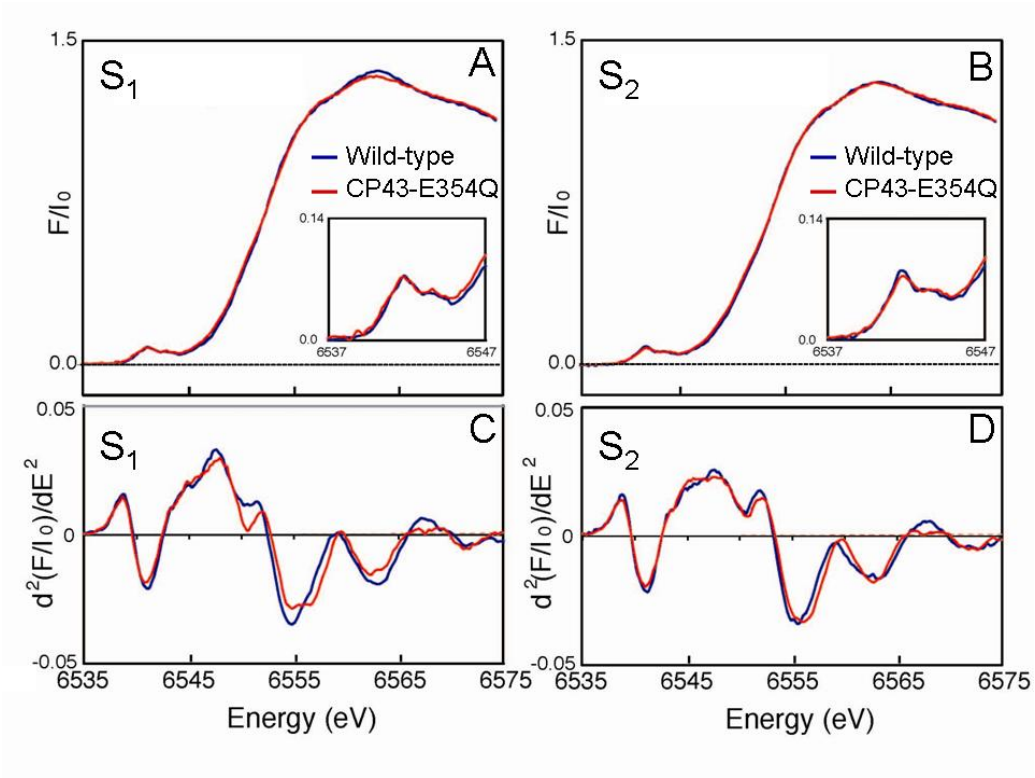

Service et al. **Figure 5**

Actual Size – Double Column Figure

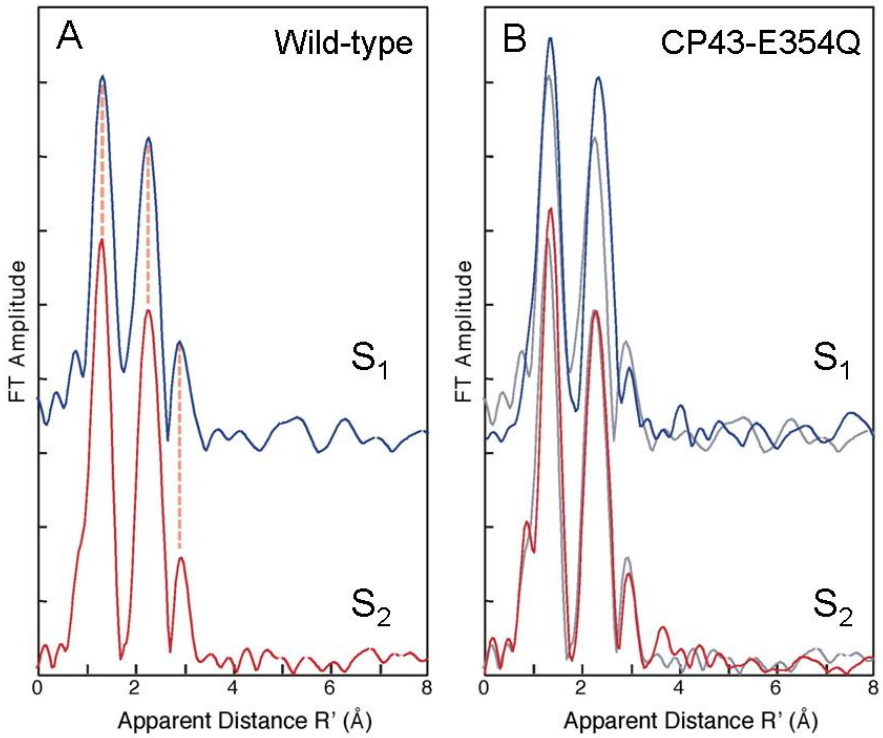

Service et al. **Figure 6**

Actual Size – Single Column Figure

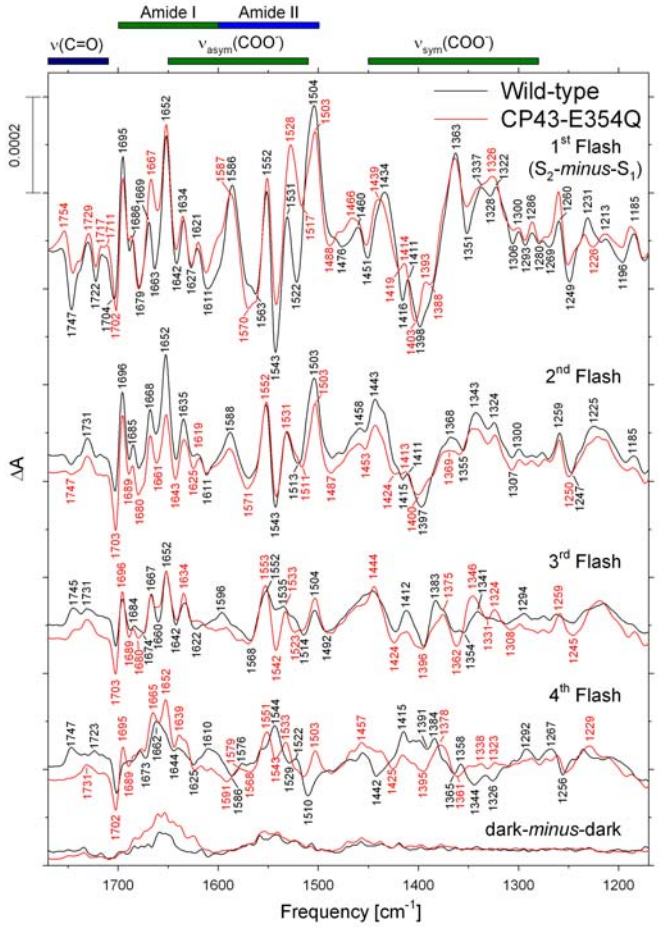

Service et al. **Figure 7**

Actual Size – Single Column Figure

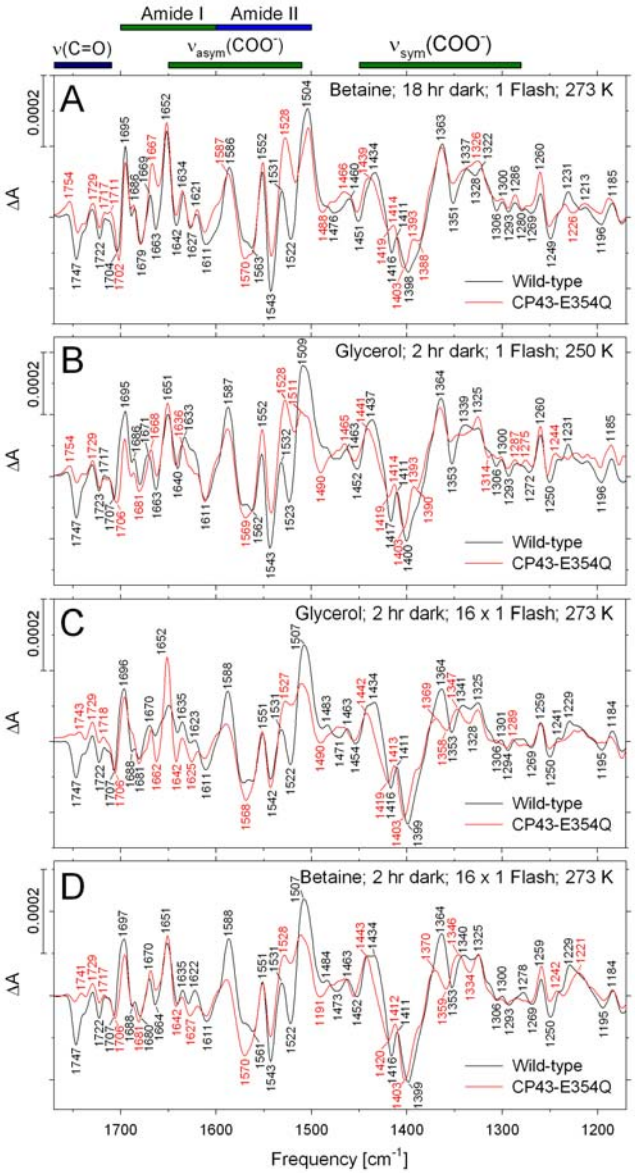

Service et al. **Figure 8**

Actual Size – Single Column Figure

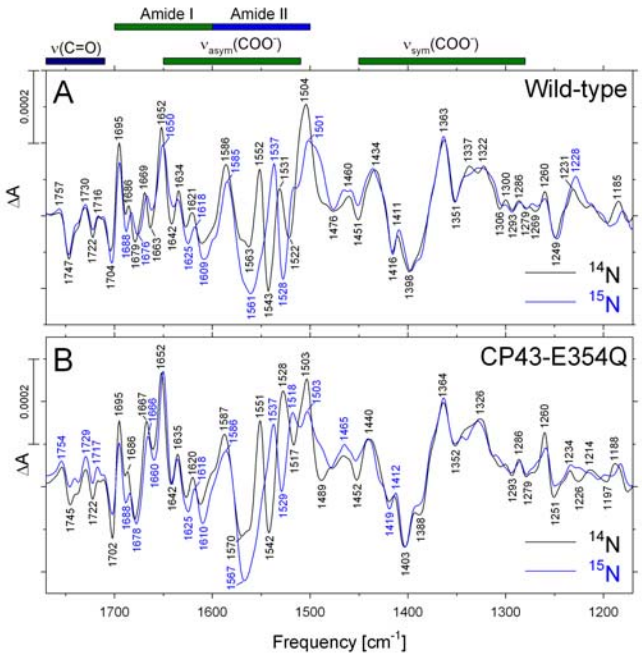

Service et al. **Figure 9**

Actual Size – Single Column Figure

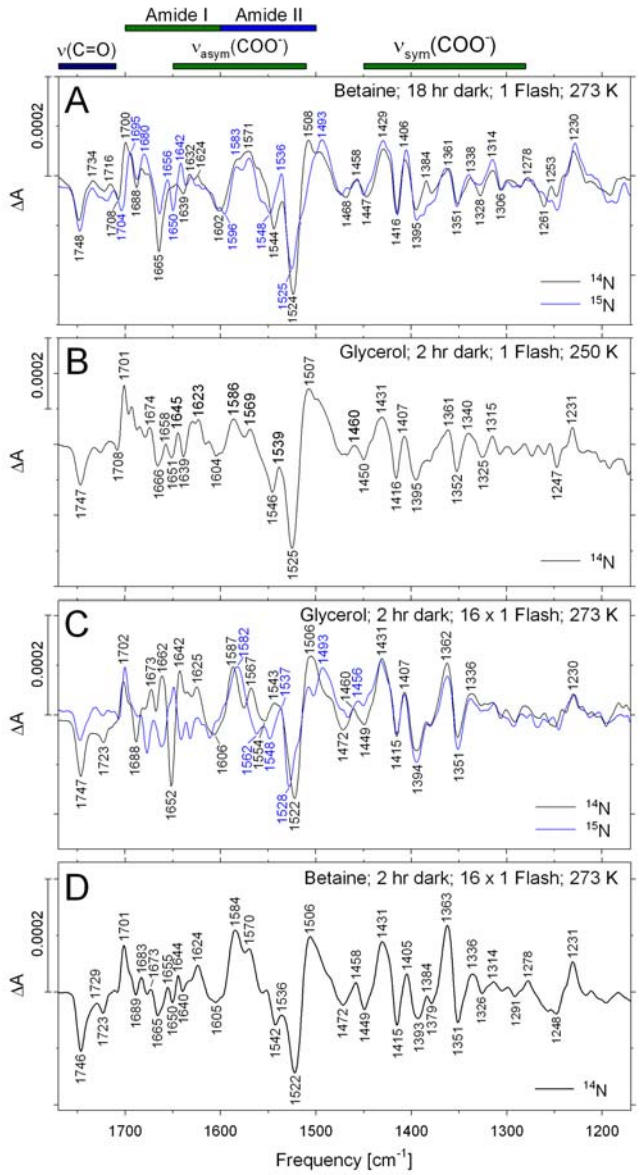

Service et al. **Figure 10**

Actual Size – Double Column Figure

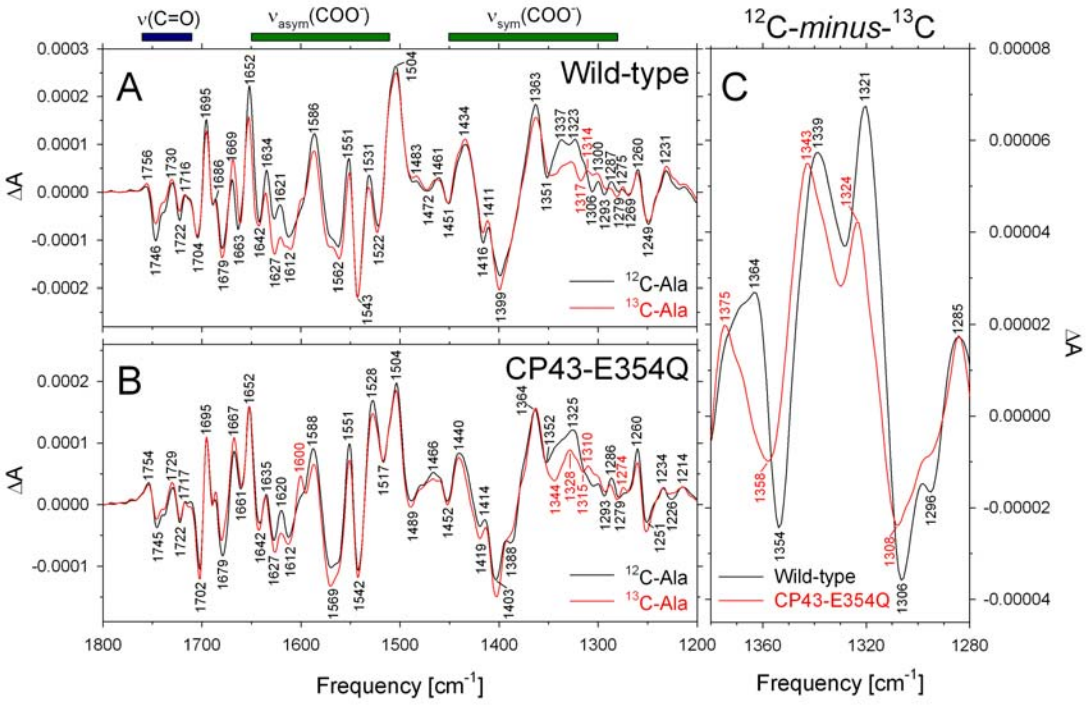

Service et al. **Figure 11**

Actual Size – Single Column Figure

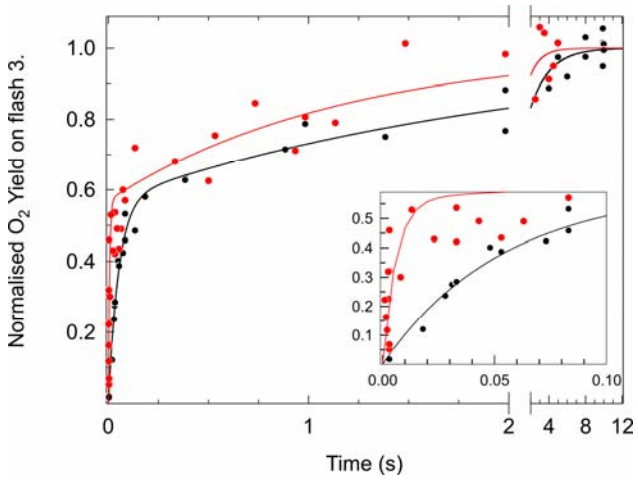

Service et al. **Figure 12**

For Table of Contents Use Only

Participation of Glutamate-354 of the CP43 Polypeptide in the Ligation of Mn and the Binding of Substrate Water in Photosystem II†

Rachel J. Service‡, Junko Yano§, Iain McConnell‖,⊥, Hong Jin Hwang¶, Dimitri Niks‡, Russ Hille‡, Tom Wydrzynski‖, Robert L. Burnap¶, Warwick Hillier‖, and Richard J. Debus‡,*

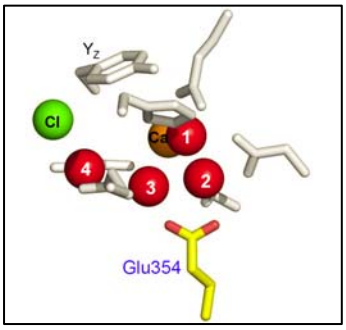

DISCLAIMER

This document was prepared as an account of work sponsored by the United States Government. While this document is believed to contain correct information, neither the United States Government nor any agency thereof, nor the Regents of the University of California, nor any of their employees, makes any warranty, express or implied, or assumes any legal responsibility for the accuracy, completeness, or usefulness of any information, apparatus, product, or process disclosed, or represents that its use would not infringe privately owned rights. Reference herein to any specific commercial product, process, or service by its trade name, trademark, manufacturer, or otherwise, does not necessarily constitute or imply its endorsement, recommendation, or favoring by the United States Government or any agency thereof, or the Regents of the University of California. The views and opinions of authors expressed herein do not necessarily state or reflect those of the United States Government or any agency thereof or the Regents of the University of California.